CNRS
Centre National de la Recherche Scientifique

INFN
Istituto Nazionale di Fisica Nucleare

Data quality and veto studies for the all-sky gravitational wave burst search in Virgo C7 Run data

M.-A. Bizouard[†], F. Cavalier[†], N. Christensen[*,♭], A. C. Clapson[†], P. Hello[†]

[*] Carleton College - Northfield MN 55057, USA
[♭] European Gravitational Observatory (EGO), Cascina, Italy
[†] LAL - CNRS/IN2P3 - Université Paris-Sud XI, 91898 Orsay, France

VIR-NOT-LAL-1390-337
Issue: 1
Date : 18th May 2007

Abstract: A gravitational wave (GW) burst search carried out in a single interferometer requires thorough understanding of the quality of the data. Indeed many sources of *glitch* type noise can mimic GW burst events. The data from the C7 commissioning run, which occurred in 2005 during a period when Virgo was operating in its final recycling configuration, has been used for an all-sky GW burst search. The origin of the highest Signal to Noise Ratio events have been studied and are now understood. A procedure to systematically identify the periods of poor quality data has been established. Furthermore, we studied the general behavior of the transient events rate in relation with external condition and the performance of the detector. We have especially demonstrated that many long transient events are actually caused by a lack of adequate alignment control. In this note we report on our detector characterization endeavors for GW burst searches that have been carried out in parallel with the tuning of the detection pipelines using the real C7 data.

VIRGO Collaboration
EGO - Via E. Amaldi - I-56021 S. Stefano a Macerata, Cascina (Pisa)
Secretariat: Telephone (39) 050 752 511 - FAX (39) 050 752 550 - e-mail perus@ego-gw.it

Contents

1 Introduction

One of the difficulties of a gravitational wave (GW) burst search is the high false alarm rate when looking for low Signal to Noise Ratio (SNR) events, and the numerous sources of transient noise (which are referred to as *glitches*) as short as the expected GW burst events that are detected by the GW burst pipelines. With an individual detector search we cannot eliminate the fake events by performing a coincidence analysis with another detector's output. It is then mandatory to identify all categories of fake events, due to the interferometer poor performance or environmental disturbances. The investigation for the reasons for possible detector malfunctioning and the sources of environmentally produced noise is very important for improving the quality of the Virgo data in the forthcoming science runs.

The study of the origin of the glitches producing the highest SNR events is one aspect of the GW burst search. Another aspect concerns the stationarity of the data. Indeed, we have noticed that from one data segment to another the trigger rate can be very different. This aspect plays an important role when setting upper limits on the GW burst rate, but in this note, we focus on the understanding of the origin of the transient noise events in the C7 data, and also on a potential instrumental veto strategy.

Thanks to the different Virgo commissioning runs, we have identified the different pre-processing steps to be followed to run a GW burst pipeline. It is especially important to identify all periods when one fundamental part of the detector was not working properly, thereby yielding abnormal behavior in the dark-fringe signal.

One of the final goals of this detector characterization endeavor was to identify the periods of data which should not be considered for the GW burst search by defining *Data Quality* (DQ) flags (see Section 4). Then, using these periods, we investigated the sources of glitches and proposed different identification means in order to veto these events. Actually, not only short transient events (glitches) have been under study, but all sources of noise which induce an excess of GW burst events. It has, for instance, been discovered that the majority of the C7 GW burst trigger excess is due to some short duration non-stationary increase of the Virgo noise in the full frequency bandwidth of the detector. Those events are not, strictly speaking, glitches.

We also addressed the veto safety issue. Indeed, vetoes must select only specific noise glitches and not a genuine GW burst event (see Section 6). The performance of the vetoes that have been used for the all-sky burst search with the C7 data are given. Several studies related to this topic have been carried out in Virgo using the C7 data [1]. We report on one of them in this note; the vetoes and DQ flags for the all-sky burst search in C7 have been based on this work.

2 Data set, channels and data selection

2.1 Data set

In this study we have used the raw data set recorded by the Virgo Data Acquisition System (DAQ) during the C7 commissioning run that took place from September 14 through 19, 2005.. The duty cycle was 65% (considering the time segments during which the interferometer was locked). The sensitivity for the run is shown in Figure 1. Figure 2 shows the maximal distance of a neutron star - neutron star(NS-NS) binary coalescence (assuming both masses at 1.4 $M_{\odot}$) detected with a SNR of 8. We also considered the calibrated strain signal in which GW burst signals have been searched. The list of time segments that have been considered, given in Appendix A, have been derived from the on-line locking web page information [2], taking into account the "Science Mode" flag which is set up by the operator during the data taking. This list of segments is actually modified according to the problem we have found in the data which prevents the application of a burst pipeline without introducing bias. This is especially the case at the end of segments due to loss of lock, as explained in Section 4. The list of auxiliary channels that have been considered for a systematic study of possible time-coincidence with the dark-fringe[1] are given in Appendix B.

[1] we call hereafter *auxiliary channel* any channel except the dark-fringe (Pr_B1_ACp in the raw data stream or the calibrated h_20kHzNo50 strain channel).

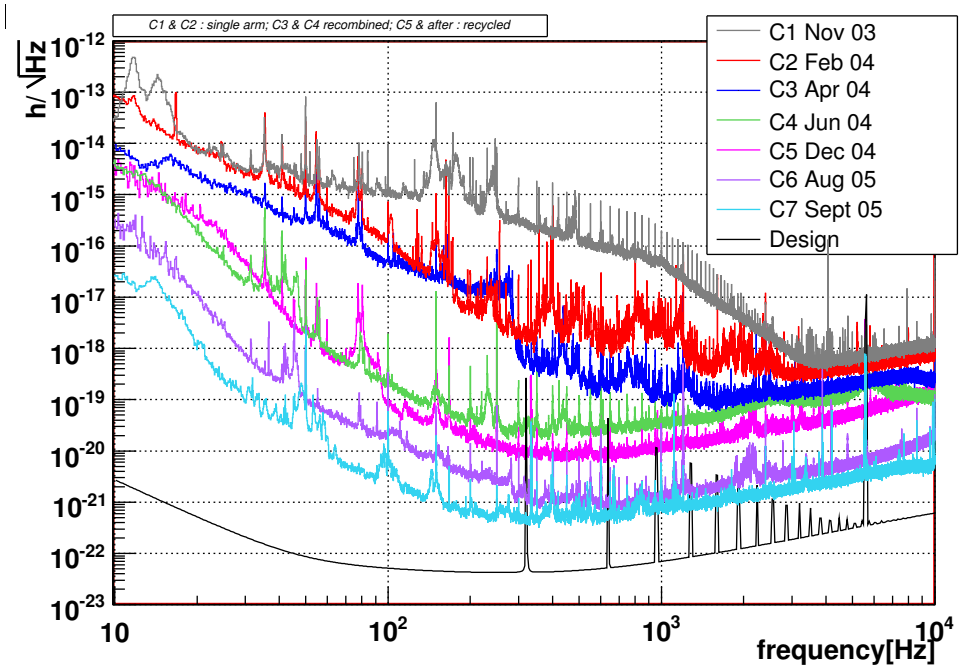

Figure 1: Sensitivity curves obtained between 2003 and 2005 during the commissioning of the Virgo detector up to the 2005 shutdown. The black curve is the nominal Virgo sensitivity curve which has been computed assuming a 10 W laser.

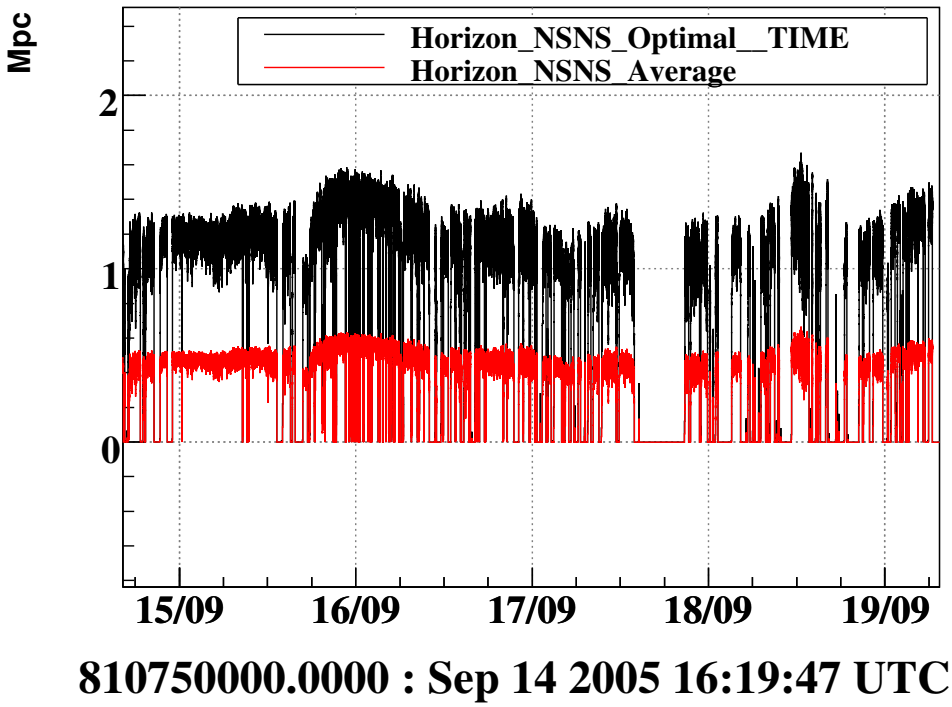

Figure 2: The Virgo C7 horizon: the maximal distance for a NS-NS binary coalescence, with each mass of 1.4 $M_{\odot}$, detected with a SNR of 8. The black curve assumes the detector is optimally oriented. The red curve averages the horizon value over all sky positions.

2.2 Signal hardware injections

Regular hardware injections of GW signals are performed during Virgo runs. With a deterministic force applied on the North Input (NI) mirror, one can induce a variation of the length of the North arm Fabry-Perot cavity which can mimic the effect of a real GW on the interferometer. These injections are called "Hardware Injections" (HI), as opposed to the software injection of signals that are done by adding a fictitious waveform to the reconstructed GW channel time series.

During C7 there were two periods of hardware injections; these included coalescing compact binary (neutron star of 1.4 $M_{\odot}$) and burst waveforms (Sine Gaussian f=920Hz, Q=15, Sine Gaussian f=460Hz, Q=15, and Gaussian σ=1ms). The HI periods occurred at the beginning and at the end of the run. Note that due to an error, three coalescing compact binaries have been injected in the middle of the run. The HI are useful and important in order to show that vetoes will not suppress any true GW events, assuming that the force applied on the mirror induces an equivalent effect in the interferometer. The GPS time of the hardware injections are given in Appendix C.

3 Pipelines

Three of the burst pipelines implemented in the BuL library [3] have been used in this study, both to look for transient events and to study the performance of possible vetoes.

- Mean Filter (MF)
  MF searches for an excess in a moving average computed on whitened data. Ten different analysis windows, with durations varying from 0.5 ms up to 10 ms, are used. The moving stride of each window is 1 bin. It has been shown that the analysis window size has to be matched on the duration of the signal to have the best detection result [4]. Note that MF behaves like a low pass filter and, given the choice of the windows' size, MF could not explore the frequency domain beyond 1 kHz. A threshold is applied on each analysis window output, producing triggers which may overlap. They are then clustered if they coincide within a time window equal to 12 times the size of the analysis window. This value corresponds to the optimal signal efficiency for the chosen threshold (SNR>5) obtained on simulated Gaussian data in which signals, such as the ones used in this study, have been injected. Finally, an information about signal frequency is provided; it is the low pass filter cutoff frequency of the window which provides the highest SNR value for the event.

- Peak Correlator (PC)
  This is a matched filter using Gaussian waveform templates [5]. The Gaussian templates have been chosen such that the minimum match is better than 99% for Gaussian peaks whose σ is between 0.2 ms and 6 ms (8 templates). That corresponds to a maximum frequency of about 900 Hz. Note that PC has been implemented using the Welch overlapping scheme [6] which optimizes the computing cost in the case of small template size. The events obtained after thresholding are then clustered using only time coincidence information.

- Exponential Gaussian Correlator (EGC)
  The complex Exponential Gaussian Correlator produces a time-frequency representation of the data by applying the correlation relation for a list of templates of the same family:

  $$\Phi_{f_0,Q_0}(t) = e^{-2(\pi f_0/Q_0)^2 t^2} e^{i2\pi f_0 t} \quad (1)$$

  with (f_0, Q_0) the central frequency and quality factor of the template.

  Template selection relies on a tiling algorithm valid for any two-parameter matched filter bank [7]. A minimal match of 99% has been used to cover the following boundaries of the parameter space: $150 \leq f \leq 1000$ Hz and $2 \leq Q \leq 16$. This results in a bank of 420 templates. An event clusterization in time and frequency is also done. More details can be found in [8].

The performance of the three pipelines have been estimated and compared to others in [10]. PC and MF are especially efficient at detecting low frequency glitches ($<$ 1 kHz) in a frequency range where many detector

glitches are expected. The EGC pipeline, focusing on higher frequency transients, has been used for an all-sky burst search.

4 Data quality flags

4.1 Definition

We first ran the MF pipeline on the GW strain signal sampled at 20 kHz ($h\_20kHzNo50$) for the list of "Science Mode" segments. Some huge SNR events (>100) have been observed in the whole set of C7 data. Obvious instrumental origins have been found for these outliers as explained below. To easily and systematically identify the periods during which one of the problems occur, we defined a list of data quality flags (DQ) that flag a data period defined with a time precision of 1 second. Following a strategy defined in the LIGO Science Collaboration (LSC), we classify the DQ in 2 categories[2]:

- Category 1: the DQ periods must be excluded before running the burst pipeline in order to prevent bad periods from spoiling the results of the GW burst search.
- Category 2: the DQ periods can be excluded *a posteriori* on the generated trigger lists.

Obviously Category 1 DQ (DQ1) periods involve the redefinition of the data segments which are used for the GW burst search. This is actually the strategy which is now used to define the segment lists posted on the web for the C7 and WSR (Weekly Science Run) runs [9].

The DQ periods and data segments are stored in ASCII files and we adopt a common format:

```
Segment index        GPS start time          GPS end time          duration     Name
```

The data segments indicate the "good" quality periods which should be used for data analysis while the DQ periods indicate the "bad" quality periods which should be excluded.

4.2 List of DQ flags for C7

Presented here is a list of identified (most of them are known for a long time) problems which induced an excess of deleterious events or very high SNR events in C7 data. One should note that this list is close to the one defined by the *on-line Detector Monitoring* system described in [12]. However, we have discovered problems that have not been detected on-line and we decided to investigate thoroughly which are the necessary DQ flags for a GW burst search.

- *EOL* (Cat. 1): During the last seconds of the segment many signals, including the GW strain signal, start oscillating, and thereby causing the loss of lock.
- *BS_SAT* (Cat. 2): The photodiodes that are used in the control of the Fabry Perot cavities, and the coil driver signals' saturation induce high SNR transients. In C7 no photodiode saturation problems have been found. Only some saturation of the Beam Splitter (BS) mirror coil drivers has been observed. During these periods, high SNR transients have been discovered.
- *PLANE* (Cat. 2): When an aircraft is flying above the interferometer at a relatively low altitude (which happens sometimes) acoustic and/or seismic noise couples into the dark fringe beam and induces a strong effect in the GW strain signal that is detected by the burst pipelines.
- *SSFS_CORR* (Cat. 2): The Second Stage Frequency Stabilization (SSFS) during C7 used the photo-diode signal Pr_B5_ACp [13]. The analog electronics of the SSFS system sometimes saturates, and that then induces incorrect control signals and consequently a misbehaving GW strain signal.

[2] the LSC defines four categories of DQ whose definition is slightly different from the ones adopted here [11].

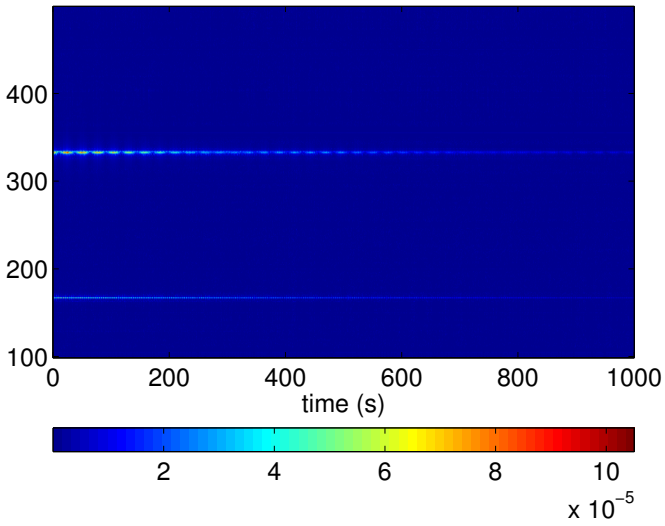

Figure 3: Spectrogram of the whitened dark fringe signal over 1000 seconds after Virgo has been relocked (beginning of segment 5). The thermal excitation of the large mirror wires (frequency 338 Hz) is observed to be decaying.

- *LINES* (Cat. 1): An excess of events with high SNR are present at the beginning of some segments. It has been found that this effect is due to the excitation of some thermal resonances of the last stage of the suspension (violin modes) (See Figure 3). These lines have been identified and their decay parameters have been measured [14].
- *HREC_BAD* (Cat. 2): An excess of events is found when the GW strain reconstruction process is facing a problem, for instance when the calibration lines are buried in the noise. When this happens the h reconstruction program sets to 0 a DQ flag stored in the data stream (SER structure Hrec_quality) [15].
- *HREC_HOLE* (Cat. 2): Sometimes during C7 a few frames or channels are missing due to some failure of the Data Acquisition system (DAQ). That induces a "hole" in the continuous time series. The burst pipelines manage properly with the presence of holes in a segment, but to properly compute the effective duty cycle we have defined a DQ flag pertaining to this issue.
- *HREC_CAL* (Cat. 1): To accurately measure the interferometer's sensitivity, some white noise is injected over a span of 5 minutes, usually occurring just before the beginning of some HI events. The presence of the white noise produces a noticeable increase of the noise level which might spoil a burst pipeline's performance. This lead us to define a category 1 DQ flag that is defined as the 5 minutes of white noise injection plus the following 5 minutes during which all resonances excited by the white noise injection damp down. Note that during C7, the white noise injection has actually been done before the start of the run.
- *HI* (Cat. 2): Hardware injections are done at specific periods of the run, and the times are flagged

4.3 DQ flags computation

4.3.1 Overflow problem

The "saturation" DQ flags (for C7: BS_SAT and SSFS_CORR DQ) have been obtained by monitoring the maximal and minimal values of the channels given in Table 1. These values (min, max) are available in the trend data files. A symetric threshold has been applied on these values (see Table 1).

DQ flag	channel name	threshold
B1_SAT	Pr_B1_d2_ACp	± 9.9 V
BS_SAT	Sc_BS_RM_CoilUL	± 9.9 V
	Sc_BS_RM_CoilUR	± 9.9 V
	Sc_BS_RM_CoilDL	± 9.9 V
	Sc_BS_RM_CoilDR	± 9.9 V
NEWE_SAT	Sc_NE_RM_CoilU	± 9.9 V
	Sc_NE_RM_CoilD	± 9.9 V
	Sc_WE_RM_CoilU	± 9.9 V
	Sc_WE_RM_CoilD	± 9.9 V
SSFS_CORR	Sc_IB_SSFS_Corr	± 9.6 V

Table 1: List of channels monitored to define the DQ periods related to signal saturation problems.

4.3.2 Thermal modes excitation

The excess of noise due to the excitation of thermal resonances associated with the suspension's last stage could be cured by removing from the data the troublesome spectral region by using an adaptive filter that can follow the damping of these lines. However, we adopted a different strategy; the N seconds during which the thermal line that has the longest decay time parameter τ ($Q = \pi f \tau$) above the noise floor are suppressed. We considered the 338 Hz thermal line corresponding to the large mirror wires' first violin mode. Following [14] we considered the band RMS (BRMS) of the dark fringe signal around this frequency in order to estimate the height of the thermal line as function of time (see Figure 4). Assuming that BRMS follows an exponential decay with time, we determined the first N seconds to be suppressed by setting a threshold on the strength of the line; the amplitude must be lower than 10% of the maximal value. The duration of the DQ periods is reported in Table 10 for each segment that is effected by this excitation problem. Note that some segments are not effected at all because the beginning of the segment does not correspond to a lock-acquisition period, as shown in Figure 4.

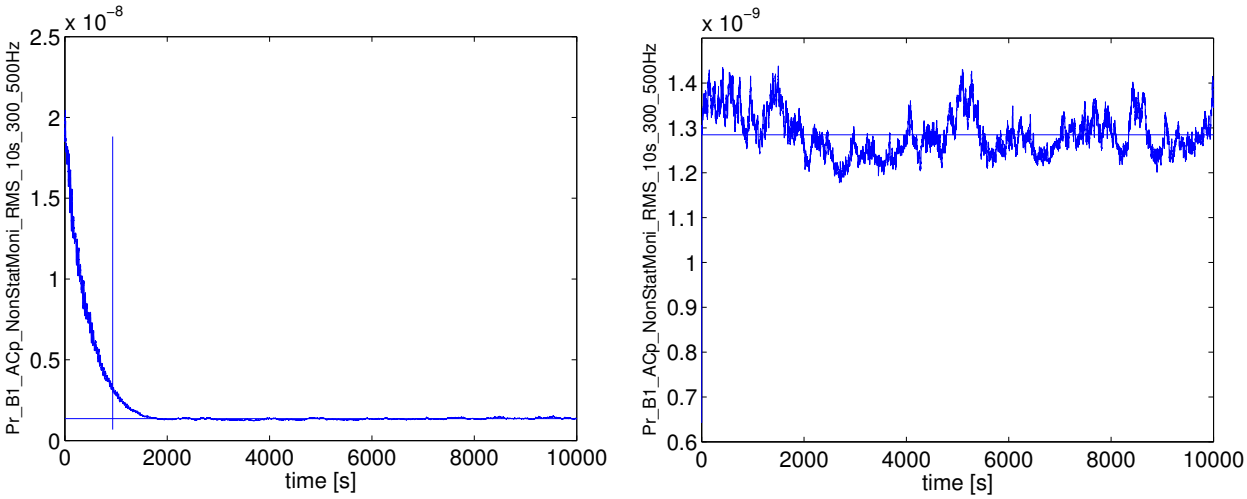

Figure 4: Band RMS of the dark-fringe signal (Pr_B1_ACp) computed over the 300-500 Hz bandwidth averaged each 10 s as defined in [16] (channel: Pr_B1_ACp_NonStatMoni_RMS_10s_300_500Hz). On the left, the damping of the large mirrors wires' violin first mode is visible in the first 1500 s of the segment whose beginning corresponds to a lock-acquisition (Segment 5). On the right plot, no excitation is visible because the beginning of this segment is far from a lock-acquisition period (Segment 12).

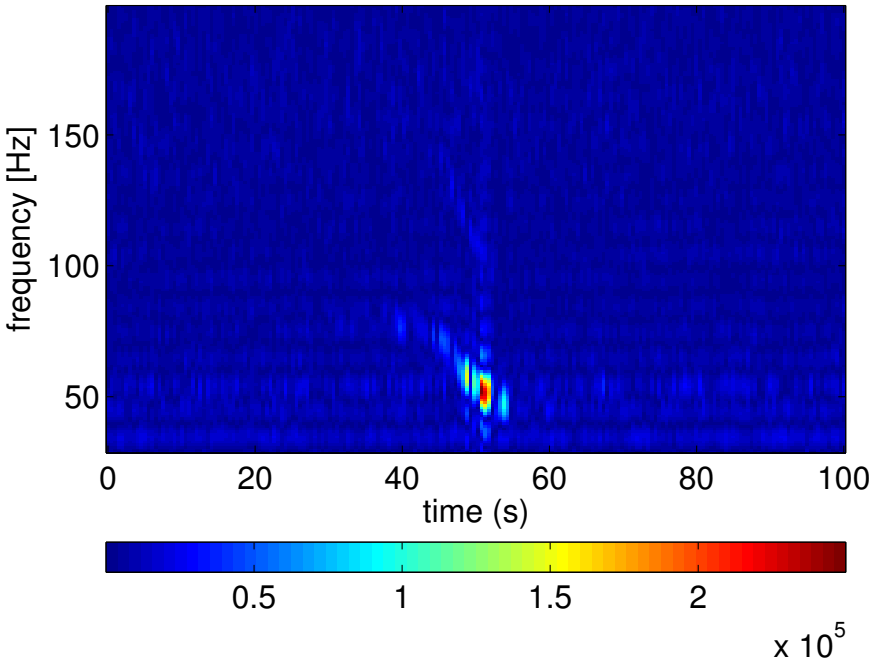

Figure 5: Spectrogram of a seismometer channel (Em_SEBDNE01) located in the North End building when an aircraft was flying over Virgo.

4.3.3 Air planes

It has been demonstrated that the passing of an aircraft at low altitude over Virgo is clearly visible in many acoustic and seismic channels and the noise couples into the dark fringe channel [17]. Figure 5 shows the spectrogram of one of the acoustic channels at a time (GPS=810805350) when an aircraft was flying nearby. The expected Doppler frequency shift is visible, which perfectly identifies the event. To find all possible "air plane events", we use the Band RMS of a seismic channel (recorded in North End building) computed between 50 and 100 Hz provided in the trend data of NonStatMoni monitoring tool (channel: Em_SEBDNE01_NonStatMoni_RMS_5s_50_100Hz). We compute the average and RMS of this channel over the full segment and set a threshold to 10 RMS. That provides time segments which are then enlarged by +/- 5 seconds in order to eliminate data periods containing "air plane" events. Two air plane events have been identified during C7.

4.4 DQ flags statistics

As already mentioned, the DQ flags of Category 1 (DQ1) were used to redefine the so-called SCIENCE segments list that has been used to perform the GW burst search in C7. The final list of SCIENCE segments is given in Appendix A. The SCIENCE segments include periods of hardware signal injections.

The DQ flags of Category 2 are combined in a global list. This DQ flag list is called COMBINED. The combination takes into account the overlap of the segments, and this is the reason why the name information of the resulting DQ flags is dropped.

The redefinition of the segments applying Category 1 DQ flags reduces the C7 duty cycle by 8%. On the other hand the dead time induced by the application of Category 2 DQ flags is only 0.8%, as shown in Table 2; this is very acceptable. The hardware signal injection periods amount to 4% of the total data set duration when the interferometer is locked.

	duration (s)	dead time
DQ1	25745	10.0 %
DQ2 (COMBINED)	2031	0.8 %
Hardware injections	10203	3.9 %

Table 2: C7 dead time due to data quality flags and the periods of signal hardware injections. The dead time is computed from the duration of the locked segments (258434 s).

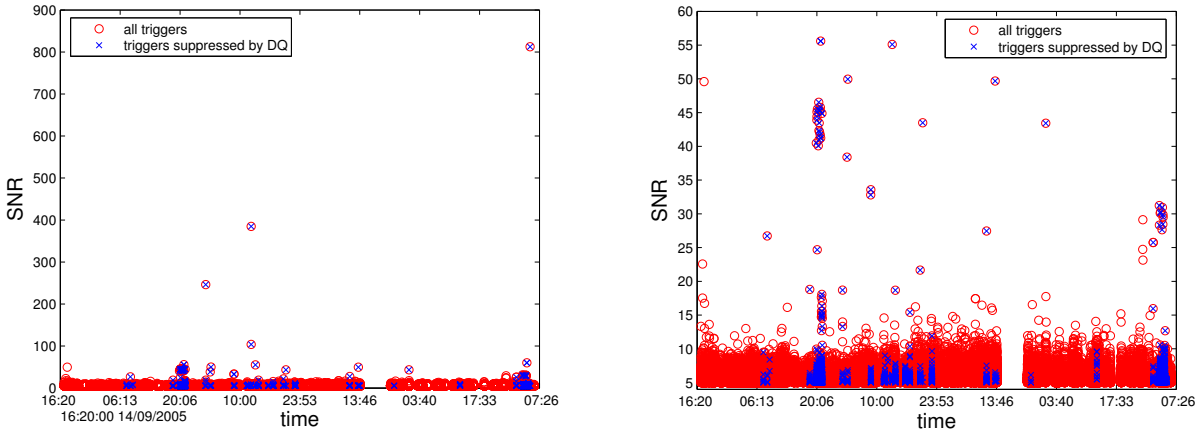

Figure 6: SNR time distribution of the MF triggers obtained on the whole C7 data set (red circles). The blue crosses indicate all the triggers which have been suppressed by applying the DQ flags defined for the C7 data set. The right plot zooms in on the SNR distribution (below SNR 50) of the remaining outliers.

	duration (s)	C7 duty cycle
ITF locked (segment > 10 minutes)	258434	65.8%
SCIENCE (DQ1 applied)	227589	57.9%
SCIENCE + DQ2 applied	225558	57.4%
SCIENCE + DQ2 applied + HI subtracted	215550	54.9%

Table 3: C7 duty cycles at different steps of the data selection for the GW burst search in the C7 data. The total duration of the C7 run is 392842 s.

Table 3 gives the effective duration of the C7 data set that has been used in the search for GW burst events in the C7 data. The duty cycle is finally reduced from 66% down to 55%. The computation of the duty cycle takes into account the fact that DQ and hardware periods can overlap. The effect of the use of the COMBINED DQ flags on the GW burst triggers detected by MF is shown in Figure 6; 550 events were suppressed, and especially all the huge SNR events (above 50) due to the use of the COMBINED DQ flags.

5 Study of the loudest glitch events

5.1 Introduction

Starting from the list of the MF and PC and EGC triggers cleaned from the main outliers due to the DQ flags, we performed an eye-scan of the remaining loudest events in order to understand their origin and hopefully find the means to automatically identify all the similar events.

Figure 7 compares the SNR histogram of the MF burst triggers for the whole C7 dataset to what should be

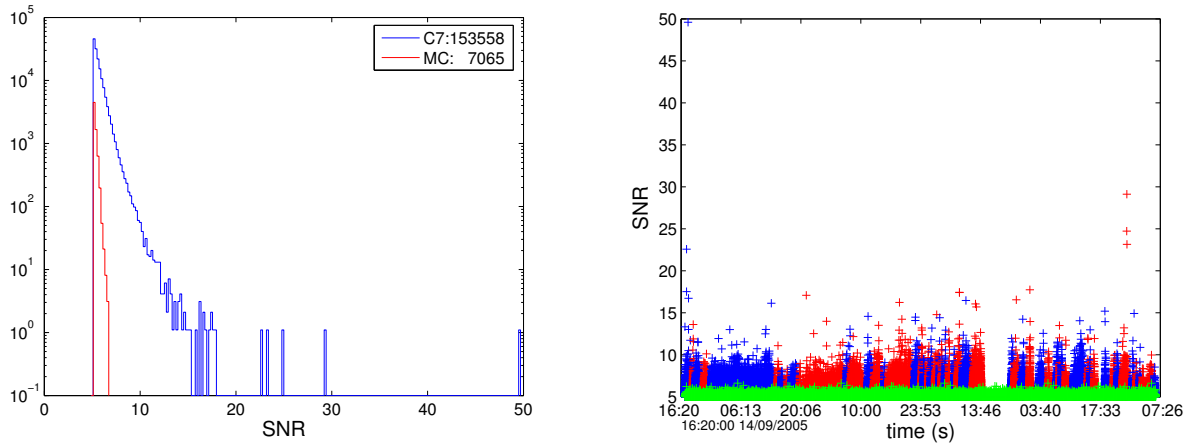

Figure 7: Left: SNR histogram of the MF triggers (blue) obtained after DQ flags have been applied. The red curve is the expectation from Gaussian and stationary Virgo noise. Right: SNR distribution of the burst triggers as function of time. The alternation of blue and red color corresponds to segments. The green points show the Gaussian and stationary Virgo noise expectation

obtained if the C7 Virgo noise were Gaussian and stationary (assuming Virgo design sensitivity). The excess of triggers (more than 20 times more events compared to Gaussian noise expectation) has been discovered to be largely due to a periodic increase of the noise floor over a large frequency bandwidth (see Section 5.2). It turned out that this effect entirely dominates all burst pipeline results for C7 and provides an excess of events over the full SNR range (not only loud events). However, aside from this excess of events, other sources of transient noise in the GW strain amplitude channel have been identified and *event by event* vetoes have been proposed.

5.2 Burst of Bursts

It has been noticed that the burst triggers are not uniformly distributed over time but seems to show up in bunches lasting up to a few seconds. Figure 8 shows the whitened GW strain channel's amplitude and its spectrogram during a data period that contains a bunch of burst triggers (around t=13 s). These events have been called Bursts of Bursts (BoB).

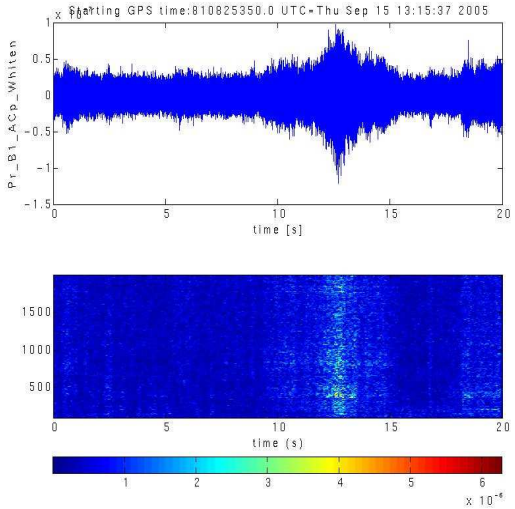

Figure 8: An example of a Burst of Burst (BoB) around t=13 s. The upper plot shows the whitened dark fringe channel amplitude as function of time, while he bottom plot is the corresponding spectrogram.

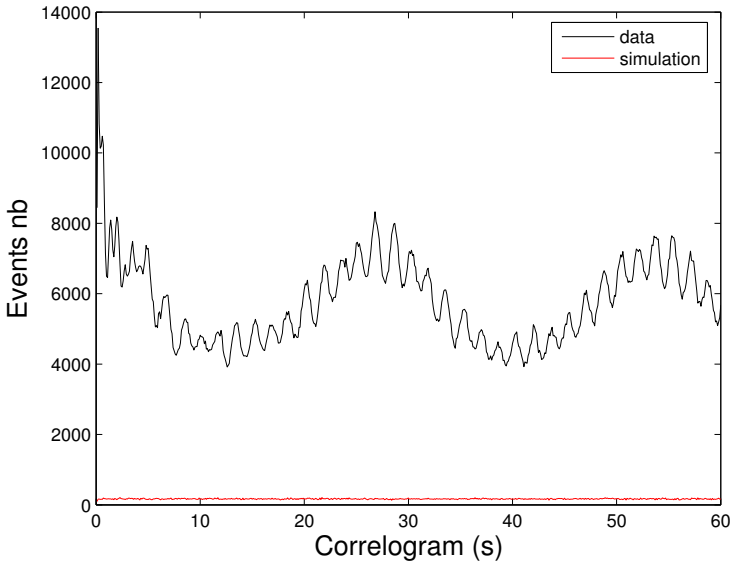

Figure 9: The correlogram of the events detected by MF with a 1 ms window. A peak around T=27s is present, with a replica at 54s. A 0.6 Hz modulation is also visible; this frequency corresponds to the pendulum mode of the last stage of the Virgo suspension.

The spectrogram shows that the event has a broadband frequency content contrary to most of the events caused by external disturbances (see for example the glitches due to Mode Cleaner and Detection Bench acoustic/seismic noise). This broadband spectral signature gave clues that helped to identify the BoBs as local increases of the noise level due to an increase of the coupling factor between the frequency noise (which is dominant at high frequency for C7 [13]) and the dark fringe channel.

We then tried to identify the cause of the variations of the coupling factor. The presence of a peak around t=27s in the correlogram of the burst events (see Figure 9) provided evidence that the residual angular motion of the mirrors could be playing a role. Indeed, 27 s corresponds to the frequency of a mechanical resonance between Filter 7 and the marionetta of the suspension that, if excited, may induce mirror angular degrees of freedom excitation [18].

Figure 10 clearly shows the correlation between BoB events and the extremal (negative) value of the θ_y angular tilt of the North End mirror (NE). The minimal coupling is obtained for $\theta_y = 1.45$ (in the plot, θ_y values are not calibrated, a factor 0.13 has to be applied to get the correct angular tilt value).

This correlation appears even more clearly on Figure 11 where the RMS (computed over 2 ms) of the dark fringe signal is plotted as function of the θ_y value of the NE mirror. This quadratic dependence is also present with a lower significance for the other angular degrees of freedom (θ_x and θ_y for all mirrors). In order to be able to identify the BoB independently from the dark fringe RMS, a quantity, hereafter called *Angles2* has been defined:

$$Angles2 = 1 + \sum_i a_i(\theta_i - \theta_i^0)^2 \tag{2}$$

where a_i and θ_i^0 have been derived from the dark fringe RMS (computed over 2 ms) using a parabolic function considering all mirrors (NE, WE, NI, WI, BS and PR).

This *Angles2* quantity indicates that, when the mirrors' angular tilt becomes large, the coupling of the dark fringe with the laser frequency noise increases. The North End θ_y angular tilt amplitude has the largest contribution, but the other mirrors contribute to the effect as well. This has been confirmed using a definition of Angles2 including only the NE θ_y variable; the rejection rate of the BoB events is then a little bit lower than when considering all mirrors' degrees of freedom in Angles2 (see Section 6.6).

Another way to monitor the dark fringe noise increase due to the laser frequency coupling variation is to consider the amplitude of the 1111 Hz line which is introduced at the level of the laser frequency control system to monitor the coupling of the laser frequency noise in the dark fringe. There is also a clear time coincidence between the 1111 Hz line amplitude height and the NE mirror large tilt. Finally, we should mention that the BoB effect, due mainly to the NE angular tilt, is at the origin of the side-bands of the 1111 Hz line that has been observed and reported in [14].

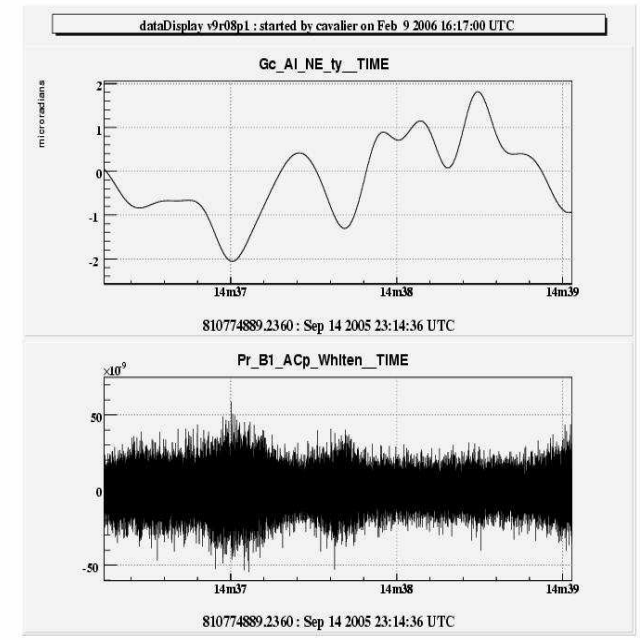

Figure 10: Above: the θ_y angular position of the North End mirror. Bottom: the corresponding whitened dark fringe signal. Each time the NE mirror takes an extreme negative value the RMS of the dark fringe increases.

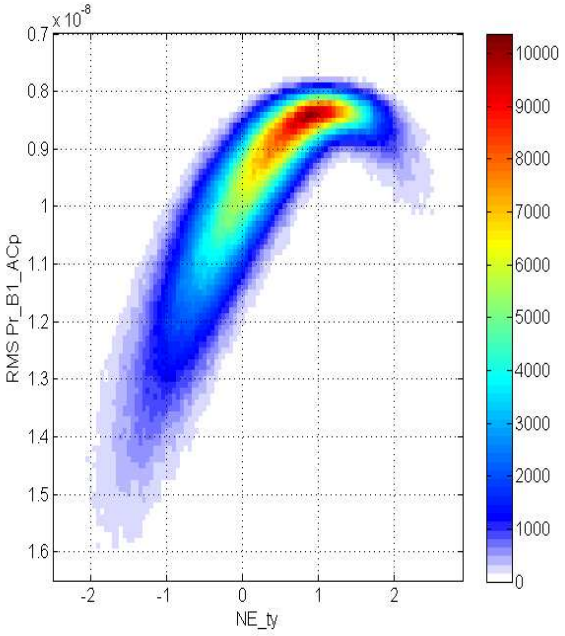

Figure 11: RMS (computed over 2 ms) of the dark fringe signal as function of the θ_y value of the North End mirror.

5.3 Other kind of glitches

Aside from the BoB events, we have identified a few sources of glitches in the C7 data that we describe briefly in the following [19].

5.3.1 Detection bench glitches

It has been seen that many high SNR burst events are coincident in time with the realignment of some quadrant photodiodes (B5 beam) located on the external bench of the detection tower. Indeed, the picomotors were generating very loud acoustic noise that couples into the dark fringe beam nearby. The external detection bench hosts the dark fringe recombined beams (B1p and B1 beams) as well as the beam reflected by the rear face of the Beam Splitter mirror (B5 beam). Quadrant photodiodes are also hosted on this bench. All these photodiodes signals are used for the control of the interferometer degrees of freedom.

Figure 12 shows that each time a quadrant is moved there is a huge increase in the signal measured by an accelerometer probe located on the detection bench. When the 2 quadrant photodiodes are not re-aligned (horizontal and vertical positions remain constant) the RMS of the accelerometer probe signal remains low. The rate of the B5 quadrant photodiodes realignment was not constant over the run; from 1 each 3 seconds reduced to 1 each 300 seconds at the end the C7 run, after the discovery of the problem (the parameters of the process responsible for the quadrant photodiodes realignment have been changed to reduce the problem).

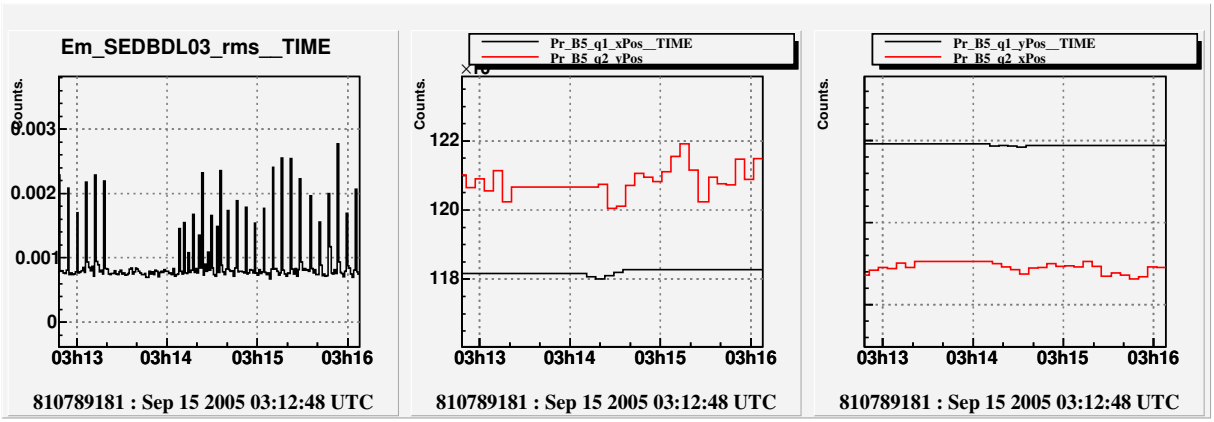

Figure 12: The left plot displays the RMS of the accelerometer output that is located on the detection bench. The RMS is computed each second. The detection bench hosts quadrant photodiodes that are aligned by picomotors, thereby generating acoustic noise. The center and right plots show the horizontal and vertical positions of 2 quadrant photodiodes. Their positions are controlled by two picomotors which are making the acoustic noise.

This acoustic/seismic noise generates glitches in the dark fringe signal whose frequency content is around 550 Hz, as shown in Figure 13. MF and PC were affected by this noise but the SNR of these events was typically not higher than SNR=10, while the EGC burst pipeline that has been used for the all-sky burst search detects these glitches with very high SNR values. An event by event veto had to be developed against these glitches.

5.3.2 Mode Cleaner glitches

Dark fringe glitches seen in coincidence with huge increase of noise in a seismic probe located in the mode cleaner building have been detected. It is suspected that the very regular seismic noise increase (each 8 minutes) was due to the air conditioning switching on and off (see Figure 14). This hypothesis could not be fully tested since just after C7 the mode cleaner building air conditioning system has been changed and the problem disappeared [20]. This source of low frequency noise mainly affects the PC and MF pipelines, and generates large SNR events. On the contrary, none of these events were detected by EGC because of the lower frequency cutoff.

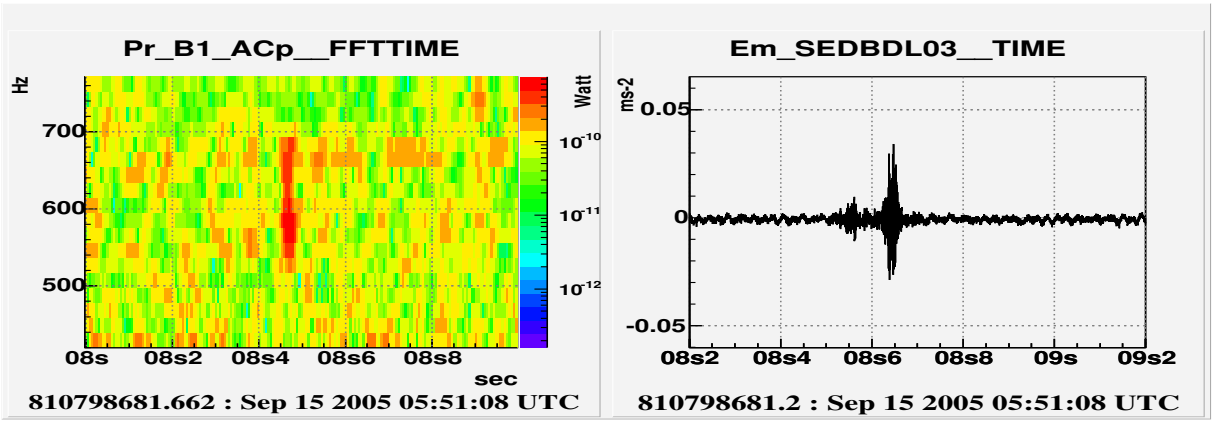

Figure 13: A spectrogram of the dark fringe signal (left) showing an excess of noise when a picomotor (that is used to align a detection bench quadrant photodiode) has been used, as displayed in the accelerometer channel (right). The acoustic noise generates dark fringe noise increase around 550 Hz.

That suggests that an event by event veto strategy must be adapted according to the tuning of the burst pipeline which is being used.

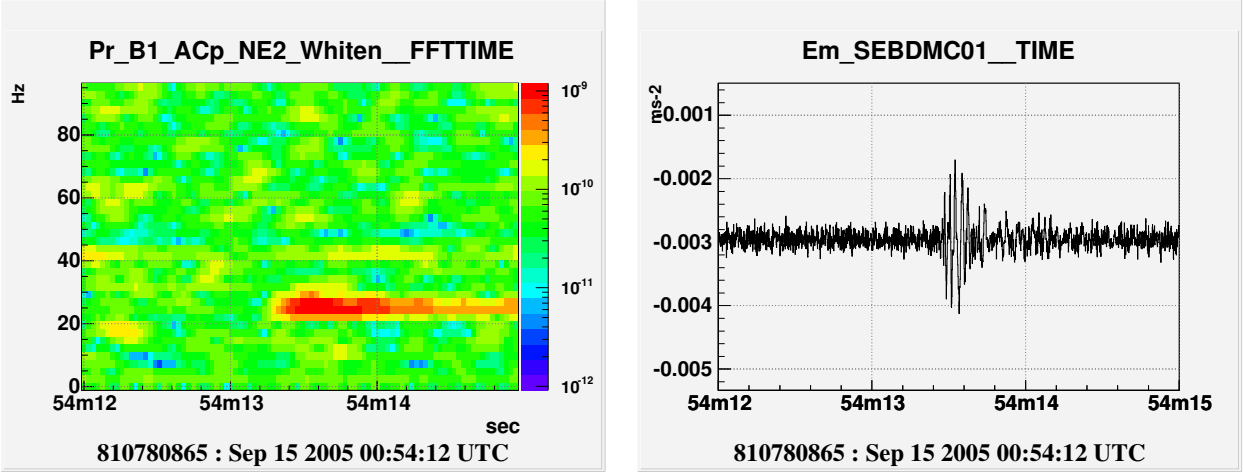

Figure 14: A spectrogram of the dark fringe signal (left) showing an excess of noise when an event is recorded in the seismic probe located inside the mode cleaner building (right). The seismic event generates a noise increase in the dark fringe signal at about 25 Hz; the glitch duration is quite long (a few hundred of milli-seconds).

5.3.3 Second Stage Frequency Stabilization control signal glitches

Other types of glitches, rarer compared to the two previous categories, have been found in the C7 data. Indeed glitches in the Second Stage Frequency Stabilization System (SSFS) correction signal have been found in coincidence with dark fringe signal glitches. Figure 15 shows an example of such kind of glitch in the SSFS correction signal. To detect these events we used MF triggers and then defined an event by event veto list to flag all the periods effected by SSFS glitches, as explained in Section 6.

5.3.4 Angular control signals oscillation

Some glitches have been found in the correction signal of the angular degrees of freedom (dof) of the mirrors. MF has been run on all the angular dof correction signals and it has been found that the loudest glitches occur

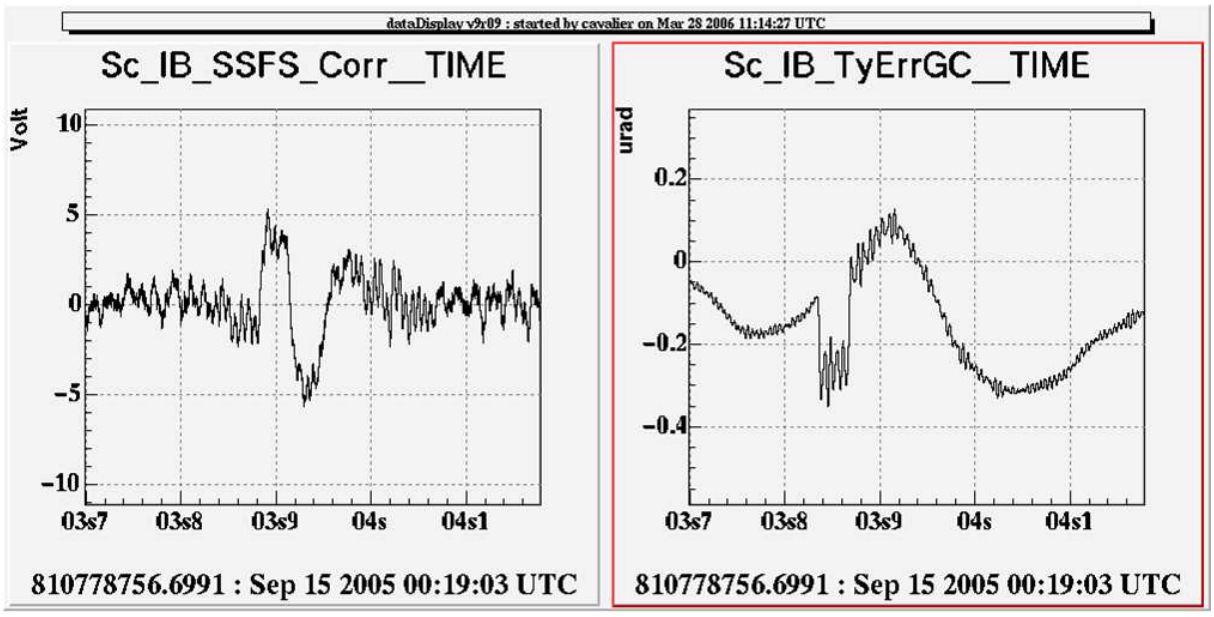

Figure 15: An example of a glitch observed in the Second Stage Frequency Stabilization correction signal.

in the West End θ_x correction signal (Sc_WE_txCorr) as shown in Figure 16. These glitches, which were rare in C7 but much more numerous in 2006 Week-end Science Runs (WSR), generate glitches in the dark fringe signal at frequencies below 200 Hz. These glitches are different from the BoB event noise. The origin has not yet been found.

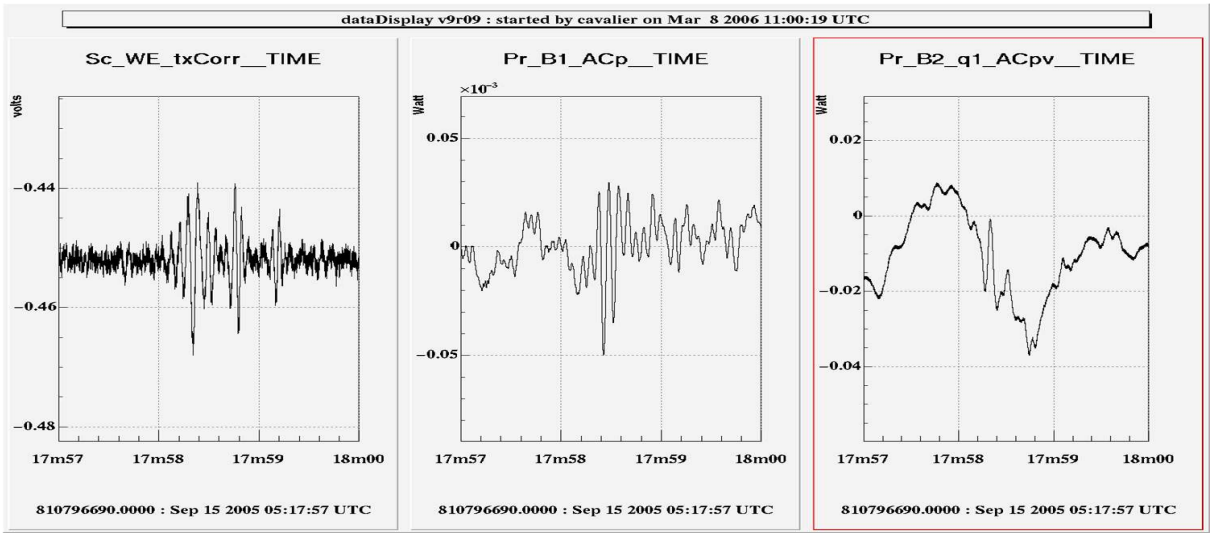

Figure 16: Glitches observed in the correction signal of the West End mirror θ_x dof. In coincidence, there is a glitch in the dark fringe channel.

5.3.5 A very strange event at high frequency

The loudest event detected by the EGC pipeline in the C7 data is a very peculiar and unique event. Only one event of this type has been found in the full run. It looks like a Sine Gaussian signal as shown in Figure 17. It matches, with a SNR of 69.7, one of the Sine Gaussian templates (f=1466Hz, Q=15.5, $\sigma = Q/\Pi f$=3.4 ms).

All environmental channels have been checked around that period using different glitch finding algorithms, including *GraphMon* a graphical scanning tool efficient at high frequencies [21]. Nothing suspect has been found in any of the environmental channels. On the contrary, a loud coincident glitch has been found in the longitudinal correction signal of the North End mirror (Sc_NE_zCorr), with a very similar waveform and at the same frequency. It has been checked that this frequency does not correspond to any known line or resonance.

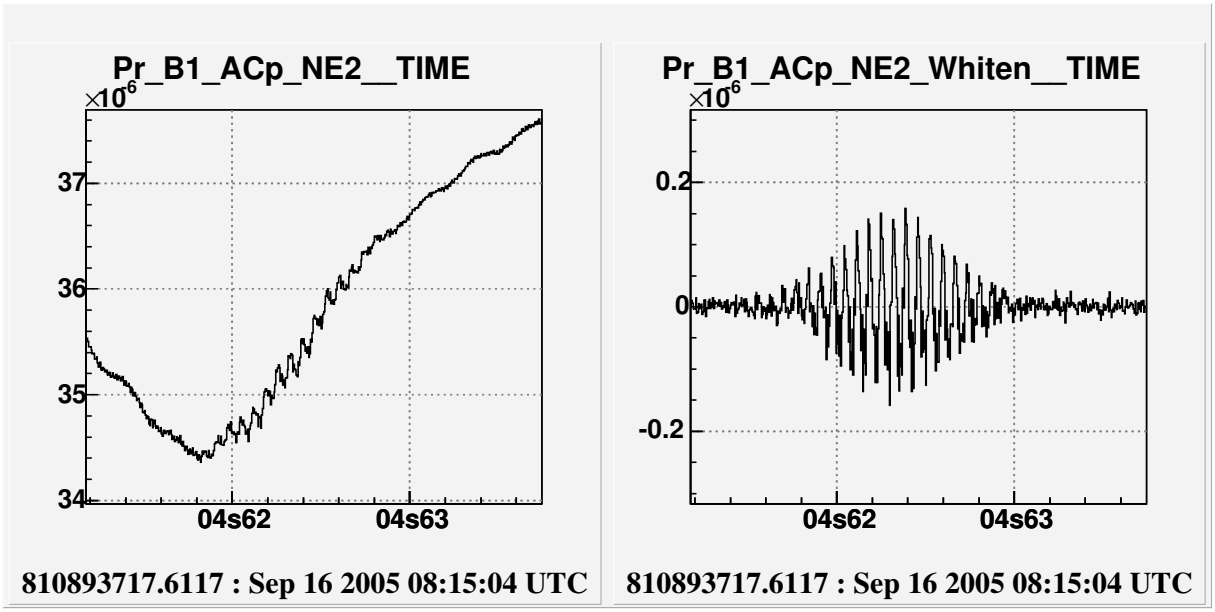

Figure 17: Time series in the raw channel (left) and the whitened raw channel (right) of the loudest event detected by the EGC pipeline in the search for GW bursts in the C7 data. This event is seen with a SNR of 69.7 at a frequency about 1466 Hz.

As the dark fringe signal (Pr_B1_ACp) is used to build the correction signal applied on the NE mirror, it is quite impossible to understand if the glitch is a dark fringe glitch or a glitch occurring in the actuator chain. However, for this particular event, the presence of a high frequency glitch in the longitudinal correction signal is incompatible with a glitch originally present in the Pr_B1_ACp channel and transmitted through the longitudinal correction since a low pass filter is applied on the correction signal (the bandwidth of the longitudinal control is smaller than 100 Hz) which should attenuate the glitch by several orders of magnitude, which is not the case. Nevertheless, as the dark fringe and the NE longitudinal correction signal are strongly coupled, we decided not to use Sc_NE_zCorr channel to design an event by event veto. We also checked that the hardware injected Sine Gaussian (f=920Hz) did not induce such a glitch in the Sc_NE_zCorr at high frequency.

Besides, the glitch is also visible in the other phase of the demodulated dark fringe signal, strongly indicating that this event cannot be a GW. Indeed, the modulation phase angle is tuned such that the effect of a GW crossing the interferometer is contained in one demodulated phase (Pr_B1_ACp), while the other (Pr_B1_ACq) should not be perturbed.

This last observation lead us to investigate a possible event by event veto based on the ratio of the SNR of time coincident triggers in the two demodulated phase signals (see Section 6.5).

6 Event by event veto studies

6.1 Introduction

After the work done to identify the origin of the glitches detected in the GW strain amplitude channel by many burst search pipelines, environmental and interferometer control channels (called auxiliary channels in the following) have been chosen to generate veto lists. This was done in order to automatically discard the burst triggers consistently associated to one of the problems mentioned above. In this study, different kinds of quantities have been considered in order to quantify the specifics of the veto:

- RMS estimated each 100 ms on the seismic probe channels: Em_SEDBDL03
- RMS estimated each 100 ms on the seismic probe channels: Em_SEBDMC01
- Triggers from the MF algorithm. Here is the list of the most interesting channels (the complete list of channels which have been studied is given in Appendix B).
  - Sc_IBS_SSFS_Corr
  - Sc_NE_txCorr
  - Pr_B5_ACq
  - Pr_B2_DC

We initially studied the properties of each veto using one segment (the longest one) to tune the different parameters and then produced the veto segment lists for the whole C7 data set. We checked that no large discrepancy between segments was present.

6.2 Definitions

The definition of an event by event veto is not straightforward and its performance actually depends on the burst pipeline that is used. In this study, we considered MF and EGC pipeline triggers to in order estimate the performance of the vetoes, as we expect there will be differences.

To build an event by event veto one has to fix the threshold applied on the auxiliary channel output (RMS or MF trigger SNR). Before that, one has to check that the coincidence between the auxiliary triggers and the burst triggers is well above the accidental rate which is expected given the statistics of the burst triggers and auxiliary channels triggers above the chosen threshold. This accidental trigger rate should follow the Poisson probability law; the number of accidental coincident events for a duration T and for a time coincidence window of size Δt is given by

$$N_{acc} = \frac{N_{GW} \times N_{Aux} \times \Delta t}{T} \tag{3}$$

where N_{GW} and N_{Aux} are the number of GW burst triggers and auxiliary channel triggers which passed the threshold on SNR. The time coincidence between burst triggers and auxiliary channel triggers is required within a time window whose size is a free parameter which has to be determined. Indeed the coincidence accuracy depends strongly on the nature of the glitch. For instance, one can see on Figure 14 that the Mode Cleaner seismic events are quite long and hence the timing accuracy of the event is not so precise. Of course, if the time coincident window is too large, the dead time generated by the veto and the accidental coincident rate will increase. Note that for the time coincidence we took into account the estimated duration of the auxiliary triggers. Indeed, we have noticed that some glitches can be large and then the peak time might not be coincident with burst trigger peak time within the time coincidence window. Taking into account the event duration information we improved the veto performance. The dead time computation takes into account the auxiliary trigger duration.

The decision of the usefulness of a veto is based on the dead time, the use percentage and the efficiency of the veto. A good veto would have a large use percentage (percentage of auxiliary veto triggers that effectively veto at least one burst trigger) and a low dead time (percentage of SCIENCE time when veto is on). Then, if the efficiency to discard high SNR burst triggers is high, the veto is determined to be very interesting. Of course, use

percentage and veto efficiency are two quantities that depend on the burst trigger population that is considered (burst triggers above a given SNR) and on the pipeline; a priori, vetoes are used to discard large SNR events. This is not the case for the veto against the BOB events whose SNR distribution is regular without a huge tail. When estimating the use percentage, one must take into account the number of accidental coincident events due to the statistics of the dark fringe signal events and auxiliary channel triggers. A good veto would have a low accidental coincident rate.

6.3 Veto list production

The final goal of this study is to provide veto lists which are list of time segments defined with a time precision given by the auxiliary channel triggers accuracy. The format of the ASCII veto list is:

```
GPS start time    GPS end time    duration    SNR_{Aux}
```

These veto lists can then be tested on burst GW triggers to estimate the performance of the veto. To build these veto lists we need to fix the following free parameters:

- SNR_{Aux}: auxiliary channel SNR threshold.
- Δt: time coincidence window size.
- T_0: time offset between the auxiliary channel and the burst triggers.

The offset T_0 parameter should, a priori, be zero in case of a real time coincidence. Actually, we used this parameter to estimate the accidental rate between the auxiliary and burst triggers. Concerning the choice of the SNR_{Aux} parameter, if the distribution of the SNR of the auxiliary triggers is bimodal, or has a long tail (as show in Figure 18), the natural choice is obvious and it should be compatible with the optimization varying all parameters (in that case it is a strong indication that the auxiliary channel is a good veto candidate).

The veto lists are generated for each SCIENCE segment. The dead time estimation is hence computed without taking into account the dead time due to the application of Category 2 DQ flags. As veto and DQ2 periods may overlap, the final dead time introduced by the two kinds of veto must be properly computed. Note that the HI signal periods are important to compare with the veto lists. That is especially the case so as to allow one to easily test the veto safety properties.

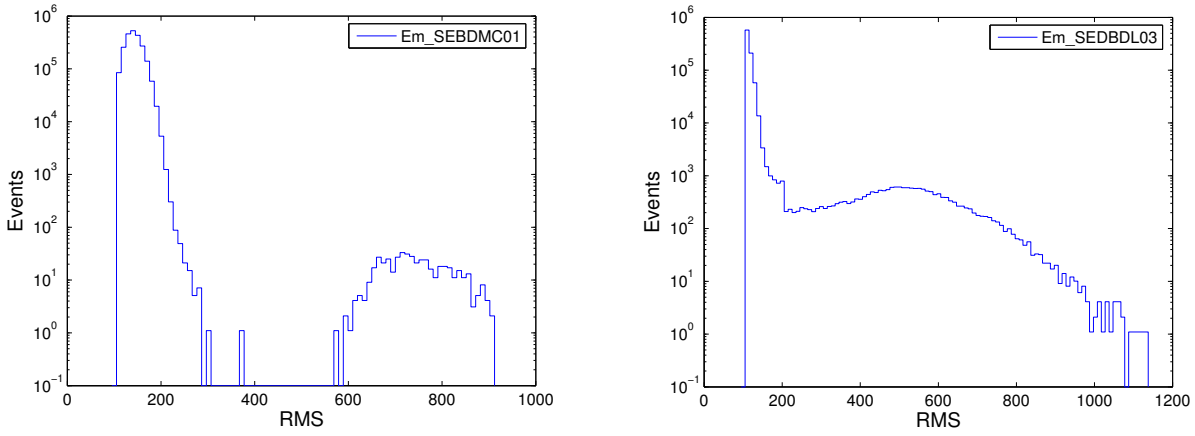

Figure 18: Distribution of the RMS of the Em_SEBDMC01 (left) and EM_SEDBDL03 (right) seismometer channels obtained on the full C7 data set. The two auxiliary channels are used to veto burst triggers due to acoustic noise that was present in the mode cleaner building (air conditioning issues, left figure) and on the external detection bench (picomotors noise, right figure).

In the case of a continuous distribution, there is no obvious choice of a veto threshold and one needs to vary the parameters and estimate the performance (use percentage, dead time and accidental rate) to determine the best choice. Here is the procedure we adopted:

- determine the offset T_0: a rather high threshold on SNR_{Aux} is fixed in order to minimize the accidental coincident rate,
- vary SNR_{Aux} and Δt (T_0 and SNR_{GW} fixed),
- compute the accidental rate, use percentage, dead time and the efficiency.

Once the parameters that maximize the use percentage and minimize the dead time were determined, we generated the veto list. To determine the starting and ending times of the veto segment we took into account the parameter T_0 which is added to the starting and ending GPS times of the segment given by the auxiliary channel whose SNR value is above the threshold SNR_{Aux}. Then, if the total duration of the veto segment is smaller than Δt, we increase it in a symmetric way such that it reaches Δt. Doing so, the duration of the auxiliary channel triggers/glitches is taken into account. Finally the dead time of the veto is computed using the final veto segment duration.

6.4 Anti-glitches veto results

6.4.1 Mode cleaner

We have first checked that triggers in the calibrated GW strain amplitude channel are in coincidence with seismic/acoustic noise in the mode cleaner building. We considered, as suggested by the distribution shown in Figure 18, all triggers for which the RMS of the seismometer channel is above 300. The main results of a coincidence analysis is shown in Figure 19 where MF dark fringe triggers have been used. One can see that if there is clearly a coincidence between MF triggers and seismic noise excess in the mode cleaner building, then the coincident MF triggers are not among the loudest triggers.

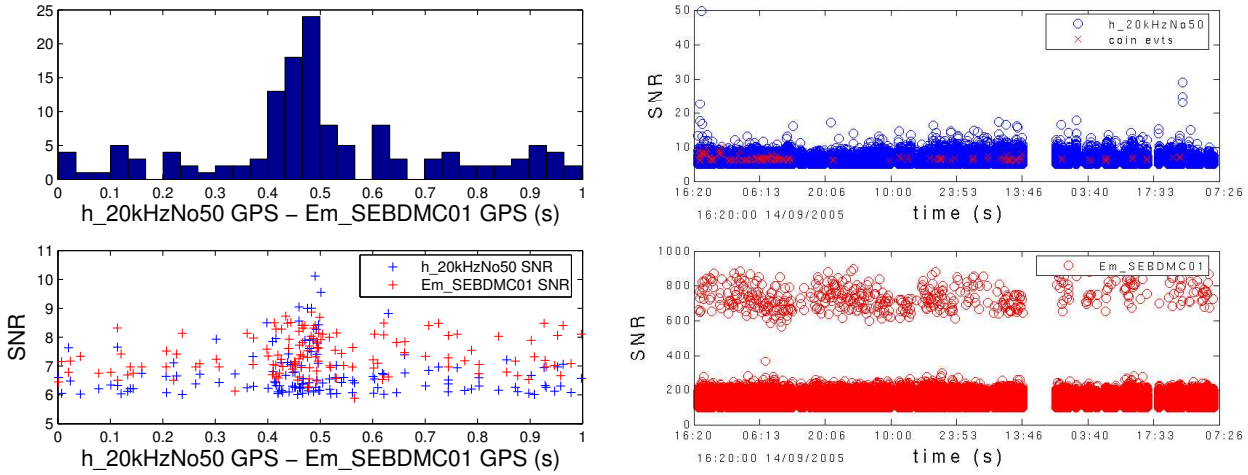

Figure 19: Left top: time difference between coincident triggers in the dark fringe and the mode cleaner building seismometer (auxiliary) channels. Left bottom: SNR of the dark fringe and auxiliary channel coincident events as function of the time difference. Right top: in blue are all the dark fringe triggers as function of time, while in red are the coincident triggers. Right bottom: RMS value of the seismometer channel as function of time.

We have estimated the time offset between the triggers from the auxiliary channels and the dark fringe signal. We have noted that the seismic noise increase in the mode cleaner building occurs systematically 500 ms before the glitch in the dark fringe channel, as displayed in Figure 20. This rather large time delay has not been

understood. The accidental coincident event rate is not negligible when considering dark fringe events with a SNR as low as 6, as shown in Figure 20. We varied the duration of the time coincidence window, and found that a Δt of 300 ms maximizes the veto efficiency. In addition, the dead time of this veto is rather low: 0.08%

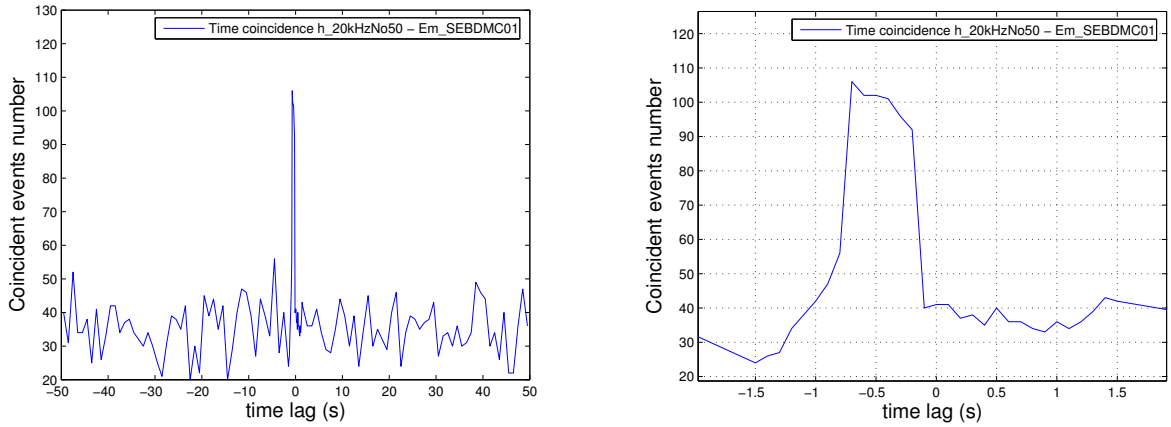

Figure 20: Left: number of coincident triggers between the mode cleaner building seismometer RMS excess and the dark fringe triggers of MF as function of a time lag. Right: zoom of the plot shown on left around the zero lag coincident value. A time offset of 500 ms clearly shows up above the accidental coincident event background.

6.4.2 Detection bench

The highest SNR events found by the EGC pipeline are mainly due to the acoustic noise generated by the realignment of some quadrant photodiodes on the external detector bench. This acoustic/seismic noise generates glitches in the dark fringe strain channel localized in frequency around 560 Hz as detected by EGC (see Figure 21).

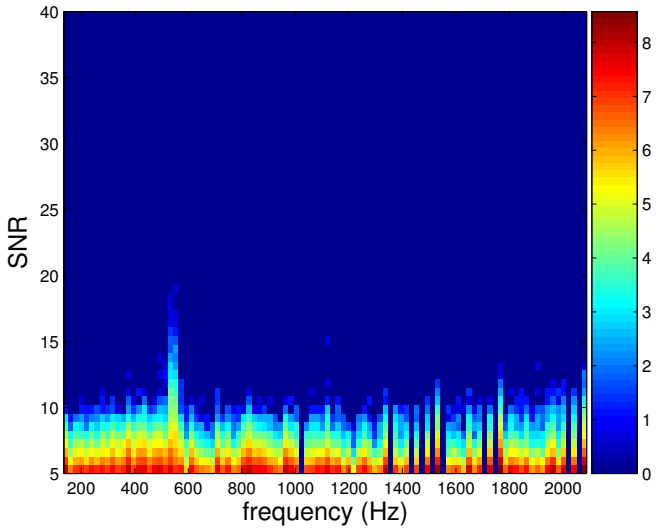

Figure 21: Trigger SNR as function of the frequency for the triggers detected by the EGC pipeline in the C7 data set. An accumulation of high SNR events around 550 Hz is clearly visible. The DQ flag of category 2 has been applied.

We applied the same procedure to detect these glitches as the one described for the mode cleaner glitches. We

used the RMS of a channel recorded by a seismometer located on the external detection bench. Contrary to the mode cleaner events, the time coincidence between the dark fringe and the auxiliary channel is lower than 100 ms which is the time resolution of the auxiliary channel used for this veto (RMS computed each 100 ms).

6.4.3 SSFS glitches

To detect the glitches in the auxiliary channel Sc_IB_SSFSCorr, we used the triggers obtained by the MF pipeline. We varied the parameters in order to optimize the efficiency of the veto using the MF triggers. Actually, this veto concerns only a very limited number of events compared to the mode cleaner and detection bench glitches. This can be seen in Figure 22, which displays the number of coincident events between the dark fringe strain channel and the auxiliary glitches. The accidental rate is rather high, but one can see an excess of coincident events when the time lag is zero. Even if the use percentage of this veto is rather low, we decided to keep that veto because it helps at suppressing rather high SNR events that are clearly due to a glitch in the SSFS correction channel.

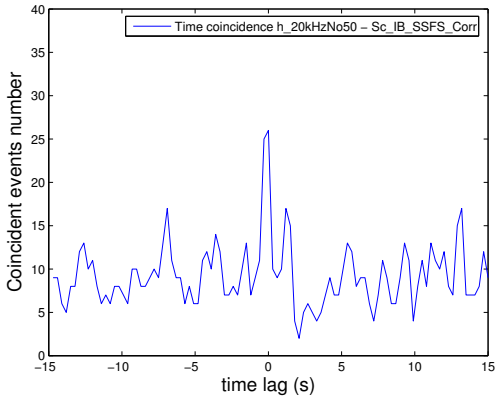

Figure 22: Number of coincident triggers between the SSFS correction channel glitches and the dark fringe strain triggers obtained by MF as function of a time lag.

6.4.4 Optical channel glitches

Some remaining loud glitches found in the dark fringe strain channel are time coincident with DC power dip recorded by the B2 photodiode. This photodiode, located on the external bench in the laser laboratory, detects light exiting the interferometer and heading back to the laser source. The light impinging on the B2 photodiode (Pr_B2_DC channel) is sensitive to the power recycling cavity length change. The origin of the power dips have not been understood. However, coincident events have been found between the dark fringe strain channel and Pr_B2_DC, well above the accidental events rate.

6.4.5 Glitch-like veto performance results on MF and EGC burst triggers

Table 4 summarizes the parameters used to define the four glitch-like vetoes that have been found to be important for the all-sky burst search. The performance obtained for MF and EGC triggers are given as function of the GW strain triggers SNR in Table 5. The use percentage, efficiency and the accidental coincident triggers-veto rate have been estimated considering 4 different categories of GW strain amplitude ($SNR_{GW} > 5$ corresponds to the full data set whereas $SNR_{GW} > 13$ selects only the highest triggers). The accidental coincident rate is estimated by adding a time lag to the veto segments list. As the accidental coincident event rate remains low, the efficiency estimation has not been corrected for the accidental coincident rate.

As expected, the veto performances are different for the 2 pipelines. It is important to note that for MF very few events have a SNR higher than 13 which is the upper value used to estimate the use percentage and efficiency of the veto.

The use percentage of the vetoes based on Em_SEBDMC01 and Sc_IB_SSFS_Corr are rather low. In addition the Sc_IB_SSFS_Corr veto dead time is not negligible (see Table 2). The Em_SEBDMC01 veto has been found to be relatively unimportant with respect to EGC dark fringe triggers, while the Sc_IB_SSFS_Corr veto has been kept despite its apparent poor performance because it helps at suppressing rather loud EGC triggers.

Auxiliary channel	T_0 (ms)	Δ_t (ms)	SNR_{Aux}	dead time
RMS Em_SEBDMC01	500	300	300	175.6 / 227589 (0.08%)
RMS Em_SEBDDL03	0	600	300	8544.4 / 227589 (3.75%)
Sc_IB_SSFS_Corr transient	0	300	6	5996.8 / 227589 (2.6%)
Pr_B2_DC transient	0	300	10	65.0 / 227589 (0.03%)

Table 4: Final choice of the three veto parameters used to build the veto lists based on quantities which detect the four main sources of glitches in the C7 data. The resulting dead time of the veto for the full C7 data set are given.

Auxiliary channel	SNR_{GW}	EGC			MF		
	threshold	Use Perc.	Efficiency	Accidental	Use Perc.	Efficiency	Accidental
Em_SEBDDL03	5	51.6%	5.3 %		20.5%	5.0%	
	8	11.6%	23.9%		1.0%	9.2%	
	10	3.5%	52.1%		0.3%	17.1%	
	13	0.6%	83.8%		0.1%	26.2%	
Em_SEBDMC01	5	26.3%	0.1%		46.5%	0.2%	
	8	2.6%	0.2%		2.1%	0.5%	
	10	0.2%	0.1%		0.2%	0.4%	
	13	0%	0 %		0.0%	0.0%	
Sc_IB_SSFS_Corr	5	29.7%	3.6%		15.7%	3.6%	
	8	3.8%	8.3%		.8%	8.2%	
	10	0.6%	9.0%		.2%	9.7%	
	13	0.1%	7.7%		0%	9.5%	
Pr_B2_DC	5	64.6%	0.1%		62.0%	0.1%	
	8	25.3%	0.4%		21.5%	1.0%	
	10	11.4%	1.0%		8.9%	2.6%	
	13	5.1%	3.4%		5.1%	9.5%	

Table 5: Use percentage, efficiency and accidental coincident event rates of the different anti-glitch vetoes which have been found useful. The use percentage and efficiency are given for the MF and EGC pipelines trigger lists obtained on the full C7 data set and for different trigger population extracted according to the dark fringe strain trigger SNR: The $SNR_{GW} > 13$ cut selects the loudest events while $SNR_{GW} > 5$ corresponds to the full trigger data set.

Figure 23 shows the effect of the veto based on the EM_SEBDDL03 channel. It clearly appears that the veto is very useful in suppressing the loudest events in the EGC dark fringe strain amplitude trigger list; however this veto pertains to only few triggers, and not the loudest, for the MF dark fringe channel triggers. Indeed, MF is not affected by the acoustic/seismic noise occurring on the external detection bench because this noise was localized in a frequency range (550 Hz) where MF is not efficient. This indicates that the use of a veto is driven by the search analysis which is carried out. Moreover, one can see on the plot showing the EGC trigger SNR as function of time, that at the end of C7, the triggers suppressed by this veto are fewer than at the beginning of the run. This is due to the fact that the source of glitches has been identified during the run and the automatic quadrant photodiodes realignment period has been increased (from one realignment each 6 seconds to one each 300 seconds).

Figure 24 shows the effect on the MF and EGC trigger distribution of the four glitch-like vetoes that have been defined for the C7 data set. Obviously the anti-glitch vetoes are very important in suppressing the loudest events of the EGC triggers while the effect of these vetoes on the MF triggers is much less impressive. 8.7% and 10.3% of the MF and EGC GW burst triggers (SNR>5) are suppressed by the four anti-glitch vetoes. But

if one considers only the trigger population with SNR > 10, then the fraction of suppressed events increases to 28% and 62.4% for MF and EGC respectively. Besides, the veto against glitches due to the mode cleaner air conditioning system is of no interest for EGC. In the all-sky burst search, this veto has not been used.

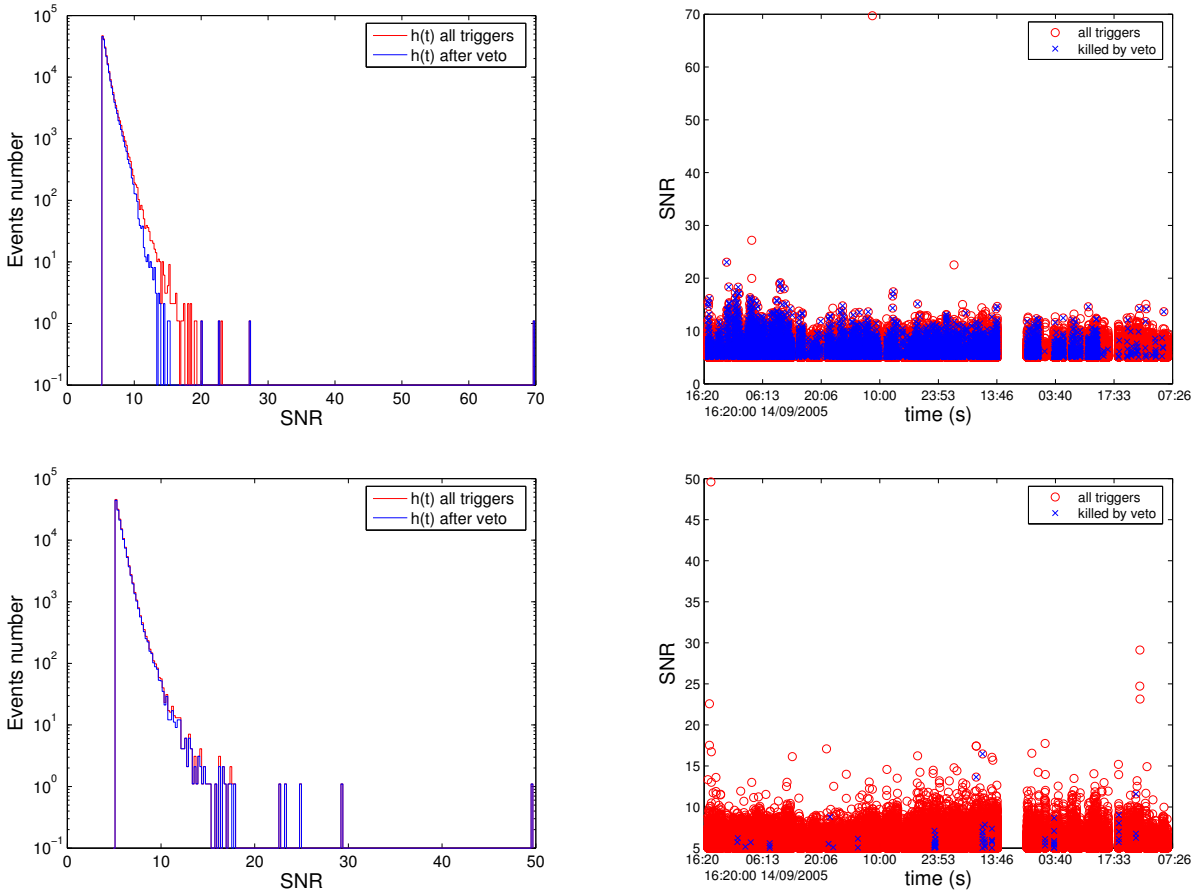

Figure 23: Left: SNR distribution of the triggers obtained in the dark fringe strain amplitude channel by EGC (top) and MF (bottom) before applying the veto based on Em_SEBDDL03 channel (red) and after the veto application (blue). Right: Same trigger distributions, but as function of the time.

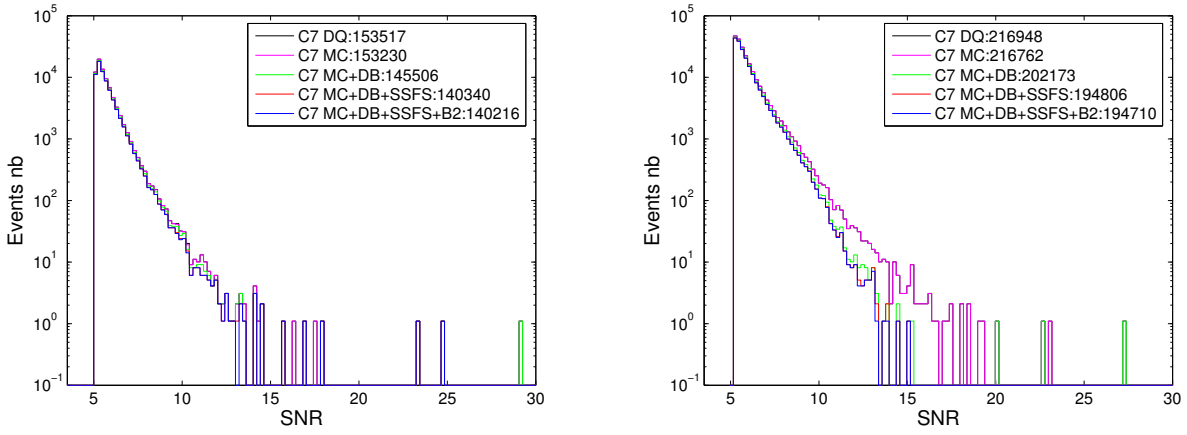

Figure 24: SNR distribution of the triggers obtained on the GW strain amplitude channel by MF (left) and EGC (right) after applying each of the four anti-glitch vetoes on the full C7 data set.

6.5 PQ veto

6.5.1 Motivation

Virgo is a power recycled Michelson interferometer which can detect a GW by measuring variations in optical signals induced by the relative displacement of mirrors when the GW crosses the detector. Frontal modulation technique are used to generate error signals used by the control of the cavities. To do so, the frequency of the laser light is modulated before entering the interferometer by an electro-optical modulator. As a consequence the phase shift associated with a relative arm length change will be detected as an amplitude modulation at the modulation frequency that is high enough (6.26 MHz) such that it will prevent the GW signal from being spoiled by laser power and electronic noises that dominate at low frequency.

The photodiode currents are demodulated in phase and in quadrature. At the output port, the in-phase signal is Pr_B1_ACp, while Pr_B1_ACq is the quadrature phase. The in-phase signal contains a priori the GW strain amplitude, provided that the demodulation phase is well tuned. An error in the demodulation phase induces a small coupling of the GW signal with the quadrature channel. However, the ratio of the GW energy seen in the two phases is expected to remain high[3]. In other words, a real GW event will be seen with a SNR in Pr_B1_ACp much higher than in Pr_B1_ACq. On the contrary, Pr_B1_ACq will be sensitive to glitches in signals which are sensitive to common mode noise. Besides, it may happen that some source of noise can affect both quadrature signals with similar strength. This is especially the case of a dust crossing the beam before the output dark port photodiode where the beam is thin [22][4].

It has been proposed few years ago in GEO[23] and LIGO[24, 25] in order to compare the energy seen in the two phases and reject false alarm events. Here we examine such a veto, namely one based on the relative size of events seen in the channels Pr_B1_ACp and Pr_B1_ACq; we call this the PQ veto. A key point of such a veto is to assure ourself that no real GW events are suppressed, and therefore one would need to develop a veto with a rather good security factor. To do so, we used the hardware signal injections to verify safety and develop the characteristics of this veto.

6.5.2 PQ veto design and results in C7 data

MF and EGC triggers have been generated for the dark fringe channels Pr_B1_ACp (ACp) and Pr_B1_ACq (ACq) and all events with SNR above 5 were considered. We then required time coincidence between the two sets of triggers using a window of ± 10 ms. The hardware injection signals were detected in the ACp triggers with an efficiency of 98% (two Sine Gaussian signals out of 93 have not been detected for unknown reason). The SNR reconstructed by EGC of the burst hardware injections is shown in Figure 25. Unfortunately, during C7, the injected SNR was not, on average, very large such that the signal energy in the ACq channel was not expected to be very high (below the pipeline threshold at SNR=5). For EGC, among the 91 detected hardware injections only 5 have a coincident trigger in the ACq phase channel within 10 ms which tends to indicate that a large fraction of the GW energy is contained in the ACp channel as expected (this is at least true for the 60 Sine Gaussian events which must be detected optimally by EGC). For MF, the situation is even worse; only one hardware injection is detected in coincidence in the two demodulation phase channels. Decreasing the SNR threshold from 5 to 4 could have increased by a small amount the detected event number, but at low SNR, the trigger clusterization algorithm fails at gathering the events properly. So we decided to keep the initial SNR threshold of 5 and consider only the EGC pipeline. The ratio between the SNR detected in the two demodulation phase channels in coincidence is:

$$\kappa = \frac{SNR_{ACp}}{SNR_{ACq}}$$

The very low event statistics (5 events detected in ACp and ACq) encourages us to stay conservative when defining the PQ veto parameters. We checked that the use of a ± 10 ms window limits the accidental coincidence event rate to 0.2 over the period of the hardware injections, which excludes the fact that among the 5 hardware events shown in Figure 26 we have one accidental association with an ACq trigger. In Figure 26, the strange

[3] We intend to estimate the ratio by using the calibration line ratio in both quadratures.

[4] In C7 data it does not seem that dust has generated some glitches in the dark fringe strain signal, while there are strong evidence that in WSR some loud burst events are in fact due to dust.

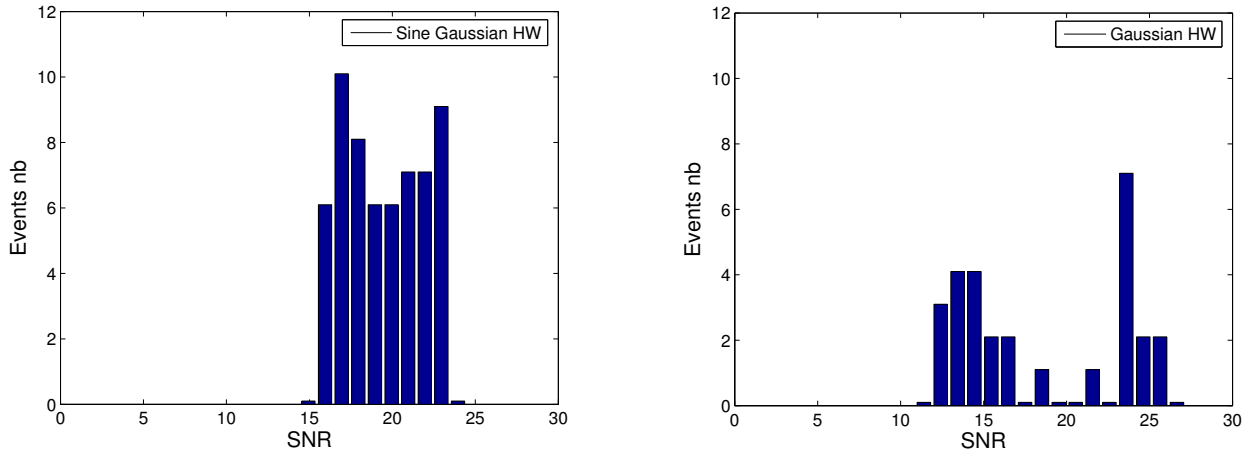

Figure 25: Reconstructed SNR of the 93 burst hardware injected signals during C7 using the EGC pipeline. Left figure: Sine Gaussian signals. Right figure: Gaussian signals.

and unique high SNR event described in Section 5.3.5 is totally isolated from the rest of the events. This event has a $\kappa = 0.42$ value and an SNR in the ACq channel of 141 which totally excludes the possibility that this event has been generated by a real GW.

This PQ veto veto aims at suppressing high SNR events in ACq channel that induce a transient in the dark fringe strain amplitude channel. That is why it is reasonable to consider only high SNR ACq triggers. A threshold Σ is applied on the SNR of the ACq triggers (SNR_{ACq}). The other veto parameter threshold Θ is applied on the ratio κ. We did not try to optimize the two parameters Σ and Θ using the use percentage and dead time criteria, but rather we keep a conservative attitude with respect to the hardware injection signals' position in the two-dimensional plane that shows the SNR of both quadratures for the coincident triggers (see Figure 26).

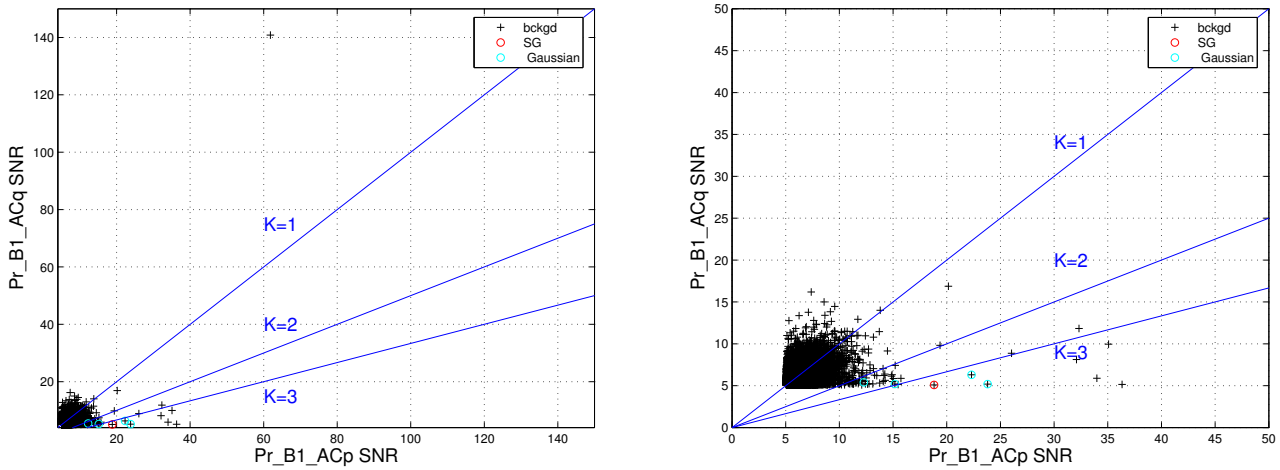

Figure 26: Left: SNR of the EGC triggers in the two quadrature demodulated channels of the output dark fringe signal: ACp (in phase) and ACq (in quadrature). The time coincidence window of the triggers seen in the two channels is 10 ms. Right: zoom of the left panel figure for events with SNR smaller than 50 in both channels.

The veto list segments have been defined as the periods during which $SNR_{ACq} > 8$ and $\kappa < 1$. All hardware injection signals pass these conditions with a safety factor since they are all below the $\kappa = 2$ line. The starting and ending times of the veto segments are given by the ACq trigger times. Nevertheless, if the ACq trigger duration is shorter than 300 ms, we enlarge on each side the duration of the veto segment in order to reach 300 ms. Figure 27 shows the number of coincident triggers in both quadratures for triggers with $\Sigma = 8$ as function of a time lag added to one of the list of triggers. One can clearly see that a majority of the triggers detected with a SNR > 8 in the ACq channel are coincident with glitches in the ACp channel.

The performance of the PQ veto is quantified in Table 6 for both the MF and EGC pipelines. The dead time amounts to 0.1% which is acceptable. This veto, in addition to eliminating the very loud and isolated event described in Section 5.3.5, suppresses a few events in the dark fringe strain channel with SNR>10. If the use percentage drops to a few percents for events above SNR >10; a few percent of events are suppressed by this veto.

Auxiliary channel	SNR_{GW}	EGC		MF	
	threshold	Use percentage	Efficiency	Use percentage	Efficiency
PQ	5	94.1%	0.5%	72.3%	0.9%
	8	25.1%	2.6%	5.8%	2.4%
	10	3.2%	2.2%	0.9%	2.6%
	13	0.5%	3.4%	0%	0%

Table 6: Use percentage and efficiency of the veto based on the ratio of SNR coincident events in the ACp and ACq channels. The use percentage and veto efficiency are given for the MF and EGC pipelines' trigger lists obtained on the full C7 data set in the calibrated dark fringe strain amplitude channel and for different trigger populations extracted according to the burst trigger SNR: The $SNR_{GW} > 13$ cut selects the loudest events while $SNR_{GW} > 5$ corresponds to the full trigger data set.

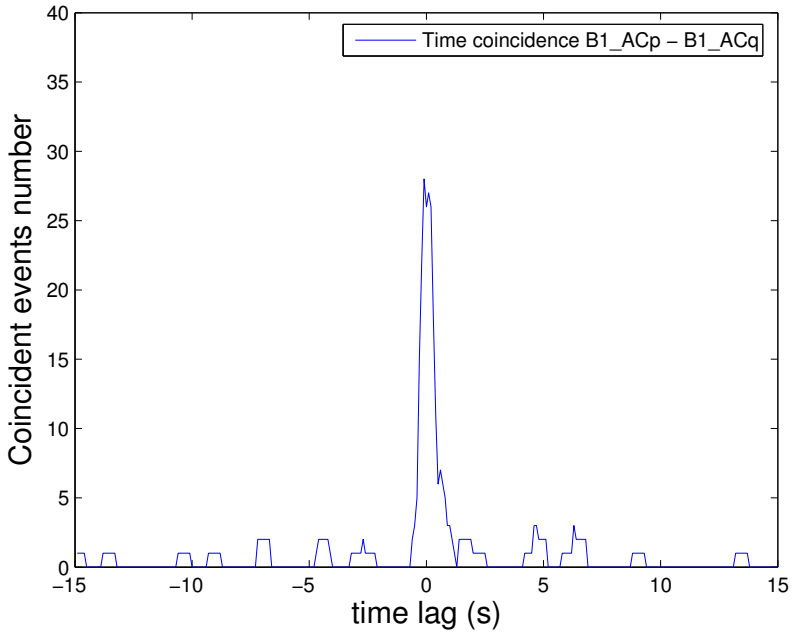

Figure 27: Number of coincident triggers in both quadrature channels for triggers with $SNR_{ACq} > 8$ as function of a time lag added to one of the list of triggers.

6.6 BoB events veto

As described in Section 5.2 the majority of the dark fringe channel burst event excess seen in the C7 data is due to a short (in time) increase of the Virgo noise. This noise increase is due to the variation of the laser frequency noise coupling in the dark fringe depending on the angular tilt of the Fabry Perot cavities. These non stationary noise periods must be eliminated from the analysis since they generate an excess of noise triggers and they correspond to periods where the Virgo sensitivity is degraded compared to the norm.

Two different quantities have been proposed to identify these periods (see Section 5.2): Angles2, which is a function of the two angular degrees of freedom θ_x and θ_y of the 6 mirrors, and the BRMS of the dark fringe channel around 1111Hz, which is the frequency of the line injected to measure the laser frequency noise component in the dark fringe channel. We investigated the possibility of building a veto using these two quantities. We estimated the performance and compared the characteristics of the two vetoes.

6.6.1 BoB event veto using the angular position of all the mirrors

The parameters used with the Angles2 function defined in Equation (2) have been determined from the data using one segment (the longest 5^{th} segment which is used as the reference segment to determine all the vetoes presented in this note). The same parameters have then been used to derive Angles2 over the full C7 data set. Angles2 is estimated at 10Hz, Figure 28 shows the Angles2 amplitude as function of time and its distribution for the full C7 run. The alternate blue and red colors indicate the SCIENCE segment boundaries. One can see that at the end of many segments Angles2 becomes large, which is actually due to the fact that the mirrors' angular tilts become large as the mirrors' control becomes unstable just before an interferometer de-lock. Furthermore, one can see that there are periods for which Angles2 has larger amplitude variations than in other segments. Actually large positive and negative values indicate that the mirrors' tilt is large and corresponds to periods where the Virgo noise increases.

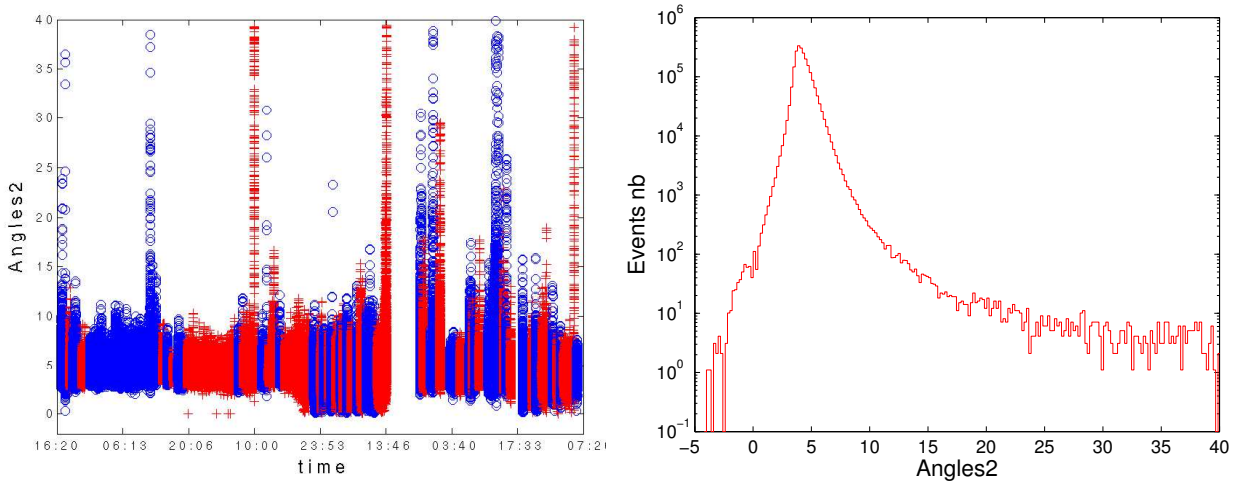

Figure 28: Left: Angles2 amplitude as function of time for the full C7 data set. The alternate colors indicate the segments. Right: Angles2 distribution which shows an asymmetric shape. Note that the histogram for values higher than 40 is not represented in the figure.

To define these noisy periods, we decided to exclude all data periods during which Angles2 is higher than T_{sup} or lower than T_{inf}. Indeed the shape of the distribution of the Angles2 variable is not symmetric as shown in Figure 28. T_{sup} and T_{inf} are two free parameters to be determined. The veto segment starting and ending times are set such that during that period, Angles2 value remains higher than T_{sup} or lower than T_{inf}. Besides, we noticed that we can improve the performance of the anti-BOB veto by enlarging the veto segment duration on each side by a quantity Δt which is the third parameter to be optimized in order to define the best performing

anti-BOB veto[5]

An important (and admittedly deleterious) feature of the anti-BOB veto is its rather large dead time, in contrast to the anti-glitch vetoes whose dead time is never higher than a few percent. In the case of the anti-BOB veto, the dead time should correspond to the amount of time during which the Virgo noise increases. Knowing that the period between 2 BoB events is 27 s, and considering 1 s long periods of non stationarity, and finally assuming that the 6 mirror suspensions are playing identical roles[6], we obtain a rough (upper limit) estimation of the BoB periods around 22%. That gives an indication of the initial values for the threshold parameters T_{sup} and T_{inf}, as well as the parameter Δt, in order to define the veto. Maximization of the use percentage and minimization of the dead time have been the criteria to choose the parameters. Unfortunately for this kind of veto, the use percentage dependence on the threshold value is rather weak. It remains high whatever the thresholds are in a large possible range of values. One can try to maximize the ratio between the number of dark fringe events suppressed by the veto and the number of false coincident events. Fixing T_{inf}=2 and Δt=300 ms we varied T_{sup} and estimated the false coincident event number by adding a time lag to the veto list segments. The curves for a few values of T_{sup} are plotted in Figure 29. One can see that, among the four tested values, the ratio is maximum for T_{sup}=5.5. We finally chose T_{inf}=2 and T_{inf}=5.4, which seems to be a good compromise. We also found that Δt=300 ms is enough to properly suppress all BoB events found by the GW burst search pipelines in the region where the noise is non stationary. Finally, the dead time of the anti-BOB veto is of 16.45% for the C7 run which is admittedly rather large for a veto. Needless to say, the probability suppressing a true GW event is not negligible. The performance of this BoB event veto is discussed in Section 6.6.3 and compared to the other anti-BoB veto described in the next Section.

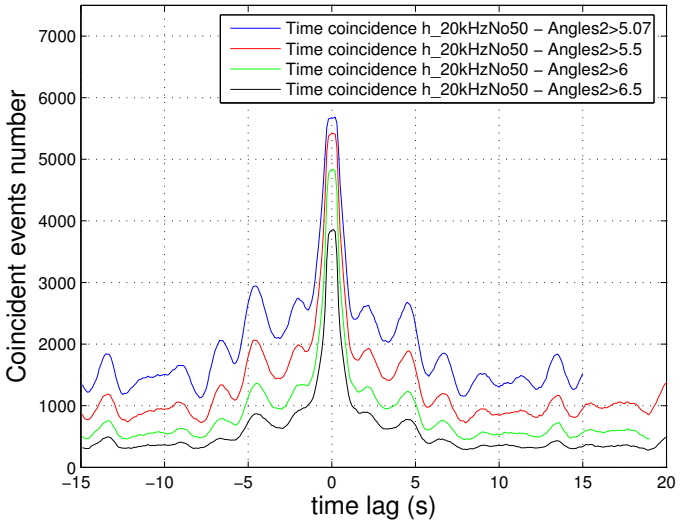

Figure 29: The number of EGC burst triggers coincident with an anti-BOB veto segment defined using the Angles2 function as function of a time lag added to the veto segments, and for different values of the upper threshold applied on Angles2 in order to define the anti-BoB veto segment list.

6.6.2 BoB event veto using the common mode noise coupling in the dark fringe

The other way to define an BoB event veto is to use the auxiliary channel for the height of the 1111 Hz line in the dark fringe (channel Pr_B1_ACp). As previously stated in Section 5.2, this line allows one to measure the common mode noise level in the dark fringe, and especially the laser frequency noise. Actually, monitoring the height of the line allows one to monitor the variation of the coupling factor between the laser frequency noise and the dark fringe signal[13]. We used the Virgo BRMSMoni software tools [26] to compute the BRMS of the dark fringe around 1111Hz over 10 Hz [1106-1116] Hz, at a sampling rate of 20Hz.

[5]Naturally, the noise increase is not instantaneous, but the excess of dark fringe channel burst triggers follows the noise increase and hence starts a little bit earlier than the moment when the noise RMS exceeds the threshold.

[6]which we know is not exact; the NE mirror angular motion amplitude was the largest.

Figure 30 shows the BRMS of the 1111Hz line as function of time and its distribution for the full C7 run. The alternate blue and red colors indicate the SCIENCE segment boundaries. As with the Angles2 distribution, one can see the non stationary features of the laser frequency noise coupling over the full run. Similar to the anti-BoB veto defined with Angles2, we used the 1111Hz BRMS to define an anti-BOB veto, but with this auxiliary channel we have only two free parameters: a threshold T_{sup} and the additional time veto duration Δt. Indeed, as shown in Figure 30, the BoB events correspond to large value of the 1111Hz BRMS. We have found that Δt=300 ms and T_{sup}=12 are adequate parameter values in order to define the veto. This then corresponds to a dead time of 16.06% for the full C7 data set.

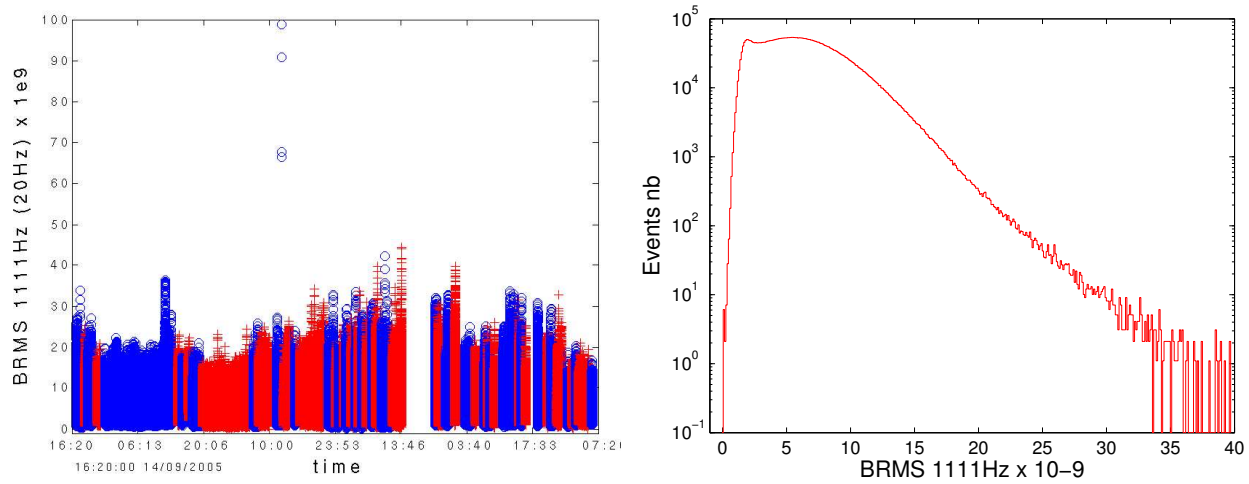

Figure 30: Left: 1111Hz BRMS amplitude as function of time for the full C7 data set. The alternate colors indicate the segments. Right: 1111Hz BRMS distribution. The 1111Hz BRMS has been multiplied by 10^9 to get unity values. Note that the histogram for values higher than 40 is not represented in the figure.

6.6.3 Comparison

Table 7 summarized the performance of the two BOB event vetoes defined using the Angles2 and the 1111Hz BRMS variables. The performances have been estimated using the MF and EGC triggers obtained in the GW burst search on the dark fringe strain amplitude channel for the full C7 data set. Recall that the dead times for the two vetoes are 16.45% and 16.06% for the Angles2 and 1111Hz BRMS anti-BoB vetoes respectively. Their effectiveness can be considered as equal.

Auxiliary channel	SNR_{GW}	EGC		MF	
	threshold	Use percentage	Efficiency	Use percentage	Efficiency
Angles2	5	86.7%	43.5%	72.9%	74.0%
	8	17.1%	76.6%	4.8%	90.9%
	10	1.3%	52.1%	0.7%	88.4%
	13	0.1%	16.2%	0.1%	81.0%
1111Hz	5	93.7%	45.4%	75.3%	74.6%
	8	16.8%	77.1%	4.8%	93.1%
	10	1.8%	54.0%	0.7%	92.5%
	13	0.1%	15.4%	0.1%	76.1%

Table 7: Use percentage and veto efficiency of the two vetoes for the BOB events. The use percentage and veto efficiency are given for the MF and EGC pipelines' trigger lists obtained on the full C7 data set and for different trigger populations extracted according to the dark fringe strain burst trigger SNR: The $SNR_{GW} > 13$ cut-off selects the loudest events while $SNR_{GW} > 5$ corresponds to the full trigger data set.

The first remarkable result to note for the anti-BoB vetoes is the high efficiency, especially for the MF triggers.

While the use percentage of the two anti-BoB vetoes is always higher for EGC triggers than for the MF triggers, the veto efficiency is higher for MF. This is because the MF triggers are mainly due to BoB events. Furthermore one can see that the efficiency is maximal if one selects events with SNR higher than 8, but decreases when the loudest events are considered. As already stated, the noise increase periods generate intermediate SNR events.

The two anti-BoB vetoes have similar performance characteristics. The use percentages are the same, while the efficiencies are a bit higher for the 1111Hz BRMS veto for the population of triggers a priori dominated by the BoB events (SNR>8). This is one argument to prefer the 1111Hz BRMS veto. The second argument is that the Angles2 function parameters have been fitted using the data of one segment of the C7 data run. The data fit seems to be valid for the full run, but the 1111Hz BRMS veto does not depend on any parameter. On the contrary, it directly makes use of the dark fringe strain amplitude channel. While the two vetoes have similar performance, they do not always exclude exactly the same periods of data, as illustrated on Figure 31, where two examples are given.

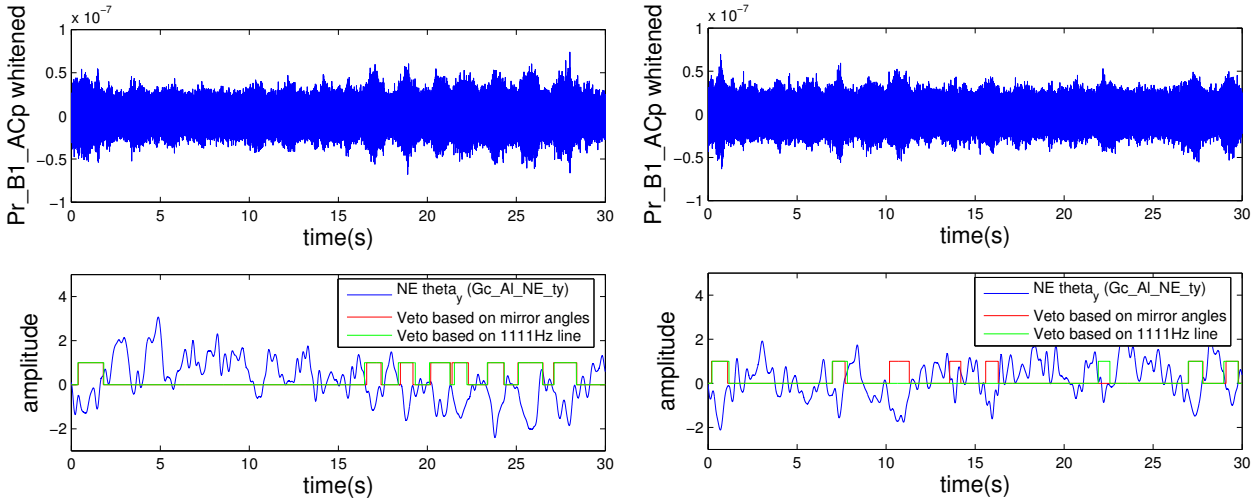

Figure 31: Two illustrations of how the anti-BoB vetoes compare, taken at two different GPS times where the Virgo noise is non stationary. Top: 30 seconds of the whitened dark fringe channel data containing many BoB events characterized, by an increase of the signal's RMS. Bottom: Renormalized NE mirror θ_y angular position as function of time (blue). Each time θ_y gets extremal lower values the noise RMS increases. The red and green curves are a representation of the anti-BoB vetoes for these 30 seconds: the value of 1 indicates that the data period is vetoed. On the left, the difference between the two vetoes is negligible, while on the right plot, the two vetoes sometimes behave differently.

6.7 Veto safety properties

The safety of a veto is of fundamental importance as we do not want to suppress any real GW event. Vetoes based and dedicated to suppress coincident glitches in the GW strain amplitude channel must be safe with respect to real GW event. The DQ flags and vetoes which suppress periods of data during which the detector is functioning poorly or where there is an excess of noise due to, for instance, the looseness of the alignment control (BoB events), can be unsafe by construction since the source of noise is independent from the effect of a real GW inside the detector. On the contrary, we must be sure that a veto based on an auxiliary channel that has some glitches remains silent when a real GW event is passing through the detector. More precisely, environmental channels such as acoustic or seismic probes are expected to be safe, whereas vetoes constructed on optical channels may be unsafe, since a GW event will generate change in photodiode signals that can be used in loop by some control feedback system. To test the safety of an auxiliary channel, one can look at the periods where HI signals are performed.

In Table 8 the number of HI events that are suppressed by the four anti-glitch vetoes is given. The important result concerns the safety of the veto based on the glitches found in the channels Sc_IB_SSFS_Corr and Pr_B2_DC, which could in principle be unsafe. The case of the PQ veto has already been discussed in Section

6.5. As expected the anti-BoB vetoes appear to be apparently unsafe, in agreement with their large dead time percentage. Actually this is true for the veto based on Angles2, while we seem to be lucky with the 1111Hz BRMS anti-BoB veto. This veto seems to be the best of all possible anti-BoB vetoes [27].

Auxiliary channel / veto	Sine Gaussian f=460Hz + Sine Gaussian f=920Hz	Gaussian width=1ms	Veto dead time
RMS Em_SEBDMC01	0/60	0/33	0.07%
RMS Em_SEBDDL03	0/60	0/33	2.4%
Sc_IB_SSFS_Corr transient	0/60	0/33	2.6%
Pr_B2_DC transient	0/60	0/33	0.02%
Angles2	7/60	6/33	16.5%
1111Hz	1/60	1/33	16.1%
PQ	0/60	0/33	0.1%

Table 8: Number of hardware injected signals suppressed by one of the vetoes discussed in this paper. The total number of hardware injections of each type is also given.

7 Use of all vetoes on MF and EGC triggers

Figure 32 shows the SNR distribution of the MF (left plot) and EGC (right plot) triggers obtained in the full C7 data set, after having applied consecutively five vetoes which have been described in this note[7]: four anti-glitch vetoes and the PQ veto. Then we compare the effect of the two anti-BoBs vetoes on the same plots (they are applied separately after the use of the other vetoes).

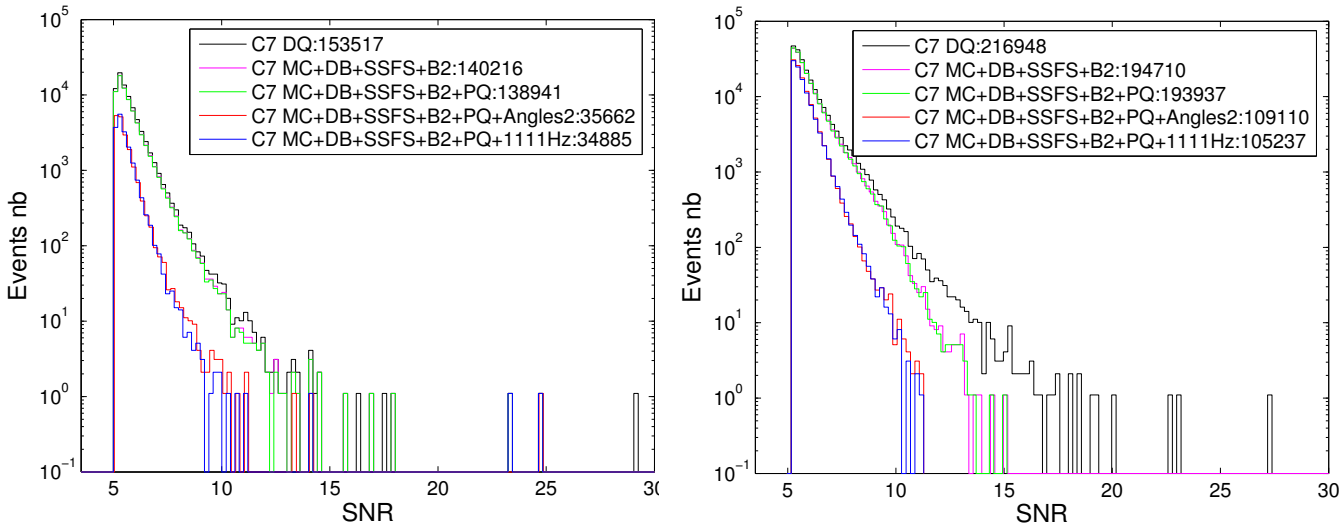

Figure 32: SNR distribution of the triggers obtained from the dark fringe strain amplitude channel by MF (left) and EGC (right) after applying, one after the other, the four anti-glitch and the PQ vetoes on the full C7 data set. The red and blue curves correspond to the use of the Angles2 and the 1111Hz BRMS anti-BoB vetoes respectively.

The four anti-glitch vetoes play an important role to suppress a large fraction of the high SNR (>10) events of EGC while for MF they play a more negligible role; 62% of the EGC triggers are suppressed and only 28% for

[7]Note that the highest SNR event is out of the scale of the plots.

MF triggers. The importance of the PQ veto is rather negligible when compared to the anti-glitch vetoes, but it is the only veto that we found to suppress the high SNR event described in Section 5.3.5.

The anti-BoB veto is of fundamental importance for both MF and EGC although its efficiency on MF triggers is extremely impressive: 75% of the MF triggers are eliminated and 92% of the loudest ones (SNR >10). The majority (more than 75%) of the MF triggers at intermediate SNR values are due to BoB events. 97% of the loudest EGC triggers (SNR > 10) are suppressed by the anti-BoB veto, such that actually there are no more events above SNR = 11.2. As already noted, the anti-BoB veto based on the 1111Hz BRMS is slightly more efficient than Angles2 veto. We decided to use the 1111Hz BRMS veto for future analyses. Finally one can note, that the MC veto is not efficient for both MF and EGC triggers. For the all-sky burst analysis, this veto has not been used.

In Table 9 we report the number of remaining events for MF and EGC after the use of the different vetoes and the number of events before the veto. The efficiency of the veto can be deduced at each step, taking into account the effect of the other vetoes already applied.

Vetoes applied	Pipeline	SNR>5 evt nb	SNR>5 red. %	SNR>10 evt nb	SNR>10 red. %
MC+DB+SSFS+B2	MF	140216/153517	8.7%	193/268	28.0%
	EGC	194710/216948	10.3%	416/1107	62.4%
MC+DB+SSFS+B2	MF	35662/138941	74.3%	23/185	87.6%
+PQ+Angles2	EGC	109110/193937	43.7%	25/402	93.8%
MC+DB+SSFS+B2	MF	34885/138941	74.9%	14/185	92.4%
+PQ+1111Hz	EGC	105237/193937	45.7%	12/402	97.0%

Table 9: Number of remaining events for MF and EGC after the use of the different vetoes and the number of events before the veto. The efficiency of the veto is given at each of the 3 veto procedure steps, taking into account the effect of the other vetoes already applied.

8 Conclusion

In this note, we described the activities which have been carried out to perform a GW burst search looking for generic and unmodeled waveform signals. One of the important outcomes of this endeavor is that the different steps to perform a GW burst search have been defined: SCIENCE segments definition, data quality flags category definition, and event by event vetoes.

The understanding of the rather noisy C7 data has been a major breakthrough in the C7 burst analysis carried out by many people, going beyond the scope of this noise study. It has been especially important to distinguish sources of real glitches from other effects, such as the non-stationary Virgo noise increases due to the mirrors' alignment control system that were not working properly during C7. This problem is now fixed and the BoB events excess is under control. For the C7 data, different kind of techniques to suppress each type of noise source have been developed: anti-glitch vetoes, a veto based on the ratio consistency test of the two demodulation phase channels of the dark output port, and a veto to identify the periods of the data where the Virgo noise increases suddenly in the full frequency bandwidth.

The application of all these vetoes allows us to reduce, by a factor 2, the number of events for all EGC triggers above SNR=5. 99% of the EGC events above SNR¿10 are eliminated, as shown in Figure 33. Only 12 EGC events above SNR=10 remain at the end. The loudest has a SNR of 11.18 and seem to be due to a short period non stationary Virgo noise increase. The final dead time induced by all the vetoes amounts to 20.2 % (overlapping veto segments have been taken into account). Note too that the final number of events remains more than two times higher that what is expected if the Virgo noise were stationary and Gaussian (see the cyan curve on Figure 33).

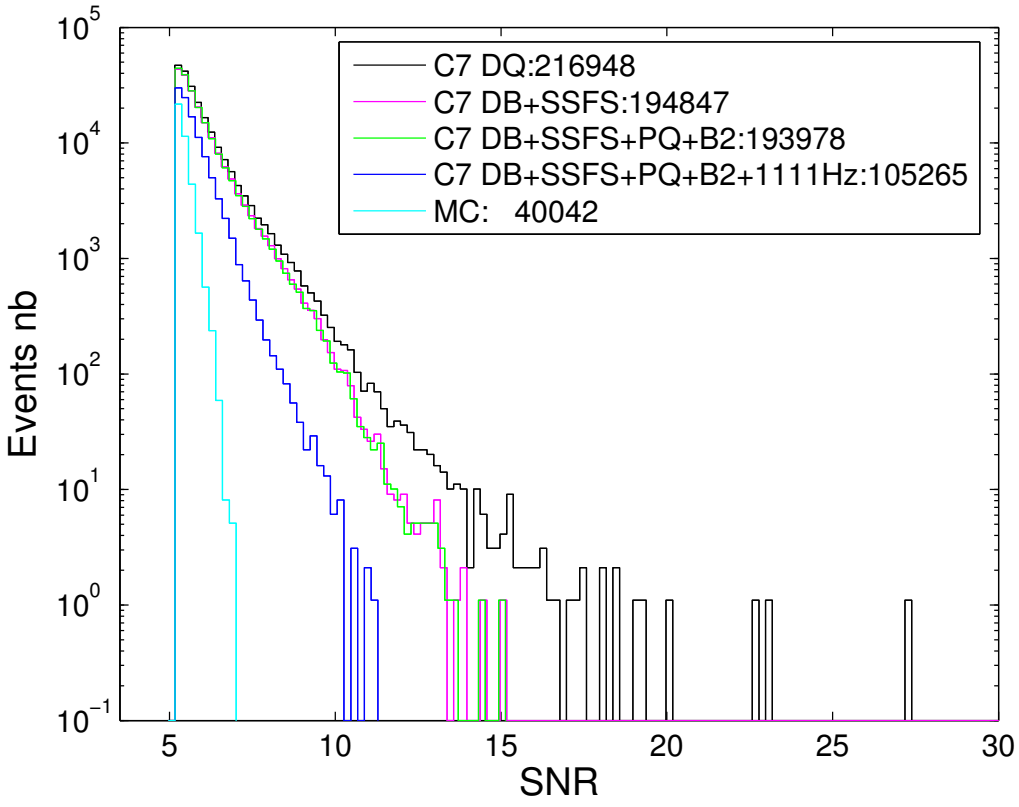

Figure 33: SNR distribution of the triggers obtained on the dark fringe strain amplitude channel by EGC after applying all vetoes on the full C7 data set. The cyan (MC) histogram is obtained using simulated stationary Gaussian noise (with the Virgo design sensitivity). The distribution is normalized such that it corresponds to the C7 duty cycle after the DQ1 flag has been applied (227589 s).

9 Appendix A

seg. ind.	GPS start (OSM)	GPS end (OSM)	LINE	GPS start	GPS end	duration
1	810752868	810758406	331	810753199	810758396	5197
2	810759784	810760516	0	810759784	810760506	722
3	810760907	810765185	878	810761785	810765175	3390
4	810768007	810771676	908	810768915	810771666	2751
5	810773996	810825448	1032	810775028	810825438	50410
6	810830530	810831539	0	810830530	810831529	999
7	810832862	810834321	626	810833488	810834311	823
8	810837843	810839130	501	810838344	810839120	776
9	810841690	810847387	0	810841690	810847377	5687
10	810848950	810885097	0	810848950	810885087	36137
11	810887399	810891259	214	810887613	810891249	3636
12	810891502	810899989	0	810891502	810899979	8477
13	810905679	810909350	0	810905679	810909340	3661
14	810910285	810915614	472	810910757	810915604	4847
15	810919476	810920123	0	810919476	810920113	637
16	810922105	810941470	953	810923058	810941460	18402
17	810943654	810948970	1015	810944669	810948960	4291
18	810949384	810951555	1021	810950405	810951545	1140
19	810951923	810952918	338	810952261	810952908	647
20	810955239	810957263	843	810956082	810957253	1171
21	810957790	810959681	111	810957976	810959671	1695
22	810960940	810964827	903	810961843	810964817	2974
23	810965241	810966056	195	810965436	810966046	610
24	810966492	810968374	768	810967260	810968364	1104
25	810969285	810970908	750	810970035	810970898	863
26	810972786	810974147	535	810973321	810974137	816
27	810977539	810979188	403	810977942	810979178	1236
28	810980215	810983032	496	810980711	810983022	2311
29	810984284	810991855	527	810984811	810991845	7034
30	810992888	811000386	615	810993503	811000376	6873
31	811025023	811027119	671	811025694	811027109	1415
32	811027857	811032476	131	811027988	811032466	4478
33	811033196	811036258	577	811033773	811036248	2475
34	811040107	811041507	537	811040644	811041497	853
35	811048032	811052500	392	811048424	811052490	4066
36	811055905	811057275	522	811056427	811057265	838
37	811062313	811064865	918	811063231	811064855	1624
38	811065394	811066121	101	811065495	811066111	616
39	811067238	811067999	121	811067359	811067989	630
40	811070588	811071434	200	811070788	811071424	636
41	811077319	811085990	158	811077477	811085980	8503
42	811089155	811089976	157	811089312	811089966	654
43	811090480	811091753	533	811091013	811091743	730
44	811094129	811095283	443	811094572	811095273	701
45	811103267	811104557	504	811103771	811104547	776
46	811110320	811112143	660	811110980	811112133	1153
47	811112621	811115740	1235	811113856	811115730	1874
48	811117296	811122252	1206	811118502	811122242	3740
49	811126559	811128223	0	811126559	811128213	1654

seg. ind.	GPS start (OSM)	GPS end (OSM)	LINE	GPS start	GPS end	duration
50	811129097	811130903	580	811129677	811130893	1216
51	811132006	811133264	369	811132375	811133254	879
52	811134411	811143076	462	811134988	811143066	7978
53	811144624	811145720	303	811144927	811145710	783

Table 10: List of C7 segments: the two first columns give the segment as defined using the "Science Mode" information (as defined during the data taking). The LINE column gives the duration of the thermal excitation present at the beginning of each segment. The last columns gives the SCIENCE segments which have been used for the burst GW search after applying the LINES and EOL DQ flags of Category 1.

10 Appendix B

Photodiodes	Control signals	Environmental probes	Environmental probes
Pr_B1_ACp	Sc_BS_txCorr	Em_ACBDCE01	Em_SEBDWE01
Pr_B1_ACq	Sc_PR_txCorr	Em_ACBDCE02	Em_SEBDWE02
Pr_B5_ACp	Sc_WI_txCorr	Em_ACBDMC01	Em_SEBDWE03
Pr_B5_ACq	Sc_NI_txCorr	Em_ACBDNE01	Em_SEDBDL03
Pr_B5_DC	Sc_NE_txCorr	Em_ACBDWE01	Em_SEDBNE01
Pr_B2_DC	Sc_WE_txCorr	Em_ACDBDL01	Em_SEDBWE01
Pr_B2_ACp		Em_ACLALL01	Em_SEIBLL01
Pr_B2_ACq	Sc_BS_tyCorr		Em_SEIBLL02
Pr_B7_DC	Sc_PR_tyCorr	Em_MABDCE01	Em_SETOBS01
Pr_B8_DC	Sc_WI_tyCorr	Em_MABDCE02	Em_SETODE01
Pr_B2_3f_d1_ACp	Sc_NI_tyCorr	Em_MABDCE03	Em_SETODE02
Pr_B2_q1_ACph	Sc_NE_tyCorr	Em_MABDNE01	Em_SETOIN01
Pr_B2_q1_ACpv	Sc_WE_tyCorr	Em_MABDNE02	Em_SETOMC01
Pr_B2_q1_ACqh		Em_MABDNE03	Em_SETONE01
Pr_B2_q1_ACqv	Sc_PR_zCorr	Em_MABDWE01	Em_SETONT01
Pr_B2_q1_DC1	Sc_BS_zCorr	Em_MABDWE02	Em_SETOPR01
Pr_B2_q1_DC2	Sc_WE_zCorr	Em_MABDWE03	Em_SETOWE01
Pr_B2_q1_DC3	Sc_NE_zCorr		Em_SETOWT01
Pr_B2_q1_DC4			Em_SEBDCE01
Pr_B2_q2_ACph	Sc_PR_zM		Em_SEBDCE02
Pr_B2_q2_ACpv	Sc_BS_zM		Em_SEBDCE03
Pr_B2_q2_ACqh	Sc_WE_zM		Em_SEBDCE04
Pr_B2_q2_ACqv	Sc_NE_zM		Em_SEBDCE05
Pr_B2_q2_DC1			Em_SEBDCE06
Pr_B2_q2_DC2	Sc_IB_FmodErr		Em_SEBDCE07
Pr_B2_q2_DC3	Sc_IB_SSFS_Corr		Em_SEBDCE08
Pr_B2_q2_DC4	Sc_IB_TraMC		Em_SEBDCE09
	Bs_IMC_D1T_DCHF		Em_SEBDCE10
			Em_SEBDCE11
	Sc_IB_txCorr		Em_SEBDCE12
	Sc_IB_tyCorr		Em_SEBDMC01
	Sc_IB_tzCorr		Em_SEBDMC02
	Sc_IB_xCorr		Em_SEBDMC03
	Sc_IB_yCorr		Em_SEBDNE01
	Sc_IB_zCorr		Em_SEBDNE02
	Sc_IB_zErrGC		Em_SEBDNE03

Table 11: List of the auxiliary channels that have investigated in the search for the sources of glitches.

11 Appendix C

Seg. ind.	GPS start	GPS end	duration (s)
10	810849565	810854570	5015
48	811122025	811122236	211
52	811135861	811140838	4977

Table 12: List of C7 hardware signal injection segments.

References

[1] E. Cuoco, M. Del Prete, N. Christensen, "Veto studies in Virgo C7 run", VIR-NOT-EGO-1390-XXX

[2] http://wwwcascina.virgo.infn.it/locking/lockmoni.htm

[3] BuL users' manual, VIR-MAN-LAL-7400-100

[4] N. Arnaud *et al*, Phys. Rev. D **68**, 102001 (2003)

[5] N. Arnaud *et al*, Phys. Rev. D **59**, 082002 (1999)

[6] P. D. Welch, IEEE Transactions on Audio and Electroacoustics **15**, 70 (1967)

[7] N. Arnaud *et al*, Phys. Rev. D **67**, 102003 (2003)

[8] A.-C. Clapson *et al*, submitted to PRD,
Ph.D. thesis, LAL, 2006, http://publication.lal.in2p3.fr/2006/theseClapson.pdf

[9] http://wwwcascina.virgo.infn.it/DataAnalysis/Segments/C7DQ.html,
http://wwwcascina.virgo.infn.it/DataAnalysis/Segments/WSRDQ.html

[10] F. Beauville *et al*, submitted to PRD, gr-qc/0701022

[11] L. Cadonati (for the LSC Collaboration), GWDAW 11, Postdam (2006)

[12] http://wwwcascina.virgo.infn.it/DataAnalysis/Quality/

[13] R. Flaminio, R. Gouaty, E. Tournefier, VIR-NOT-LAP-1390-313

[14] I. Fiori, N. Christensen, E. Cuoco, F. Paoletti, G. Vajente, "Analysis of frequency lines in C7 run", VIR-NOT-EGO-1390-339

[15] http://wwwcascina.virgo.infn.it/DataAnalysis/Calibration/hrec.html

[16] G. Vajente, Virgo noise group, http://wwwcascina.virgo.infn.it/DataAnalysis/Noise/doc/Noise_meetings/2006/20060919/Vajente_190906_NonStatWSR1.ppt

[17] F. Fidecaro, Virgo data analysis, http://wwwcascina.virgo.infn.it/collmeetings/presentations/2006/2006-02/DataAnalysis/

[18] G. Losurdo, *private communication*

[19] F. Cavalier, Virgo data analysis, http://wwwcascina.virgo.infn.it/collmeetings/presentations/2006/2006-06/DataAnalysis/

[20] I. Fiori, Virgo data analysis, http://wwwcascina.virgo.infn.it/collmeetings/presentations/2006/2006-04/DataAnalysis/

[21] H. Bantilan, N. Christensen, GraphMon tool

[22] R. Schofield, http://www.ligo.caltech.edu/docs/G/G040391-00.pdf

[23] K. Koetter, I. Heng, M. Hewitson, K. Strain, G. Woan and H. Ward, Class. Quantum Grav. **20** S895-S902 (2003)

[24] C. Hanna (for the LSC Collaboration), Class. Quantum Grav. **20** S895-S902 (2003)

[25] N. Christensen (for the LSC Collaboration), Class. Quantum Grav. **22** S1059-S1068 (2005)

[26] D. Verkindt *et al*, BRMS of the Detector Monitoring tools

[27] D$^{\rm r}$ Pangloss, *private communication*